Article:
Angulo, Rodolfo José, Fonseca Giannini, Paulo César, de Souza, Maria Cristina et al. (2026) Ages of different shell species associated to vermetid bioconstructions remains and their implications on Mid-to Late-Holocene Brazilian sea-level curves. Quaternary Science Reviews. 109788. ISSN: 0277-3791

https://doi.org/10.1016/j.quascirev.2025.109788

Ages of different shell species associated to vermetid bioconstructions remains and their implications on Mid- to Late-Holocene Brazilian sea-level curves

Rodolfo José Angulo*[a], Paulo César Fonseca Giannini[b], Maria Cristina de Souza[c], Augusto Luiz Ferreira Junior[d], Thiago de Freitas Toniolo[e], Jesús Alberto Salas Rangel[f] and Ed Garrett[g]

*Corresponding author: Rodolfo José Angulo, fitoangulo@gmail.com

[a] Laboratório de Estudos Costeiros, Departamento de Geologia, Universidade Federal do Paraná, Brazil, fitoangulo@gmail.com

[b]Instituto de Geociências, Universidade de São Paulo, São Paulo, Brazil, pcgianni@usp.br.

[c]Laboratório de Estudos Costeiros, Departamento de Geologia, Universidade Federal do Paraná, Brazil, cristinasouza2527@gmail.com

[d]Pós-Graduação de Genética Evolutiva e Biologia Molecular, Universidade Federal de São Carlos, Brazil, augustolferreirajr@gmail.com

[e]Instituto de Geociências, Universidade de São Paulo, São Paulo, Brazil, thiago.freitas.toniolo@gmail.com

[f]Instituto de Geociências, Universidade de São Paulo, São Paulo, Brazil, jesussalas@usp.br

[g]Department of Environment and Geography, University of York, ed.garrett@york.ac.uk

Abstract

Vermetid bioconstructions have been widely used as Holocene paleo-sea level indicators along the Brazilian coast, due to their abundance and accuracy, especially in the case of *Petaloconchus varians* (d'Orbigny 1841). Most age determinations for this species have been performed using conventional ^{14}C dating of bulk bioconstruction samples. However, this type of sample may contain several types of carbonate or carbonaceous impurities, including remains of other organisms such as mollusks and barnacles, which can affect the reliability of the age. This work compares previous conventional ^{14}C ages of vermetid bioconstruction bulk samples with ^{14}C AMS ages of shells from different species dated individually. The objectives are: i. to establish the relationship among the ages of different species in order to reveal the direction or tendency of past sea-level changes; ii. to evaluate the error in dating bulk samples; iii. to analyze the reliability of the ages obtained from each species, based on aspects such as purity, alteration and neomorphism. The dating results obtained for fossil shells of different species were in agreement with the relative ages expected based on the

observed spatial relationship between them. *Tetraclita stalactifera* parietal plates were older than overgrowing vermetids shells, and shells of the bivalve *Leiosolenus* af. *bisulcatus* in life position, which perforate the bioconstruction, were younger. The ages of individual shells were older than those obtained by dating bulk vermetid bioconstructions, and this difference increased with the age. Taking the paleolevels previously determined for the studied samples and using the revised ages reported here, we infer that relative sea level in southern Brazil was more than 2 m above present between 6000 and 7000 cal aBP. The differences in ages between bulk and individual shell samples highlight that paleo-sea levels inferred from bulk vermetid remains and respective Holocene sea-level curves need revision. More data for separate species are therefore necessary to improve the accuracy of Holocene sea-level curves from Brazil. Furthermore, methodological care must be taken to avoid the influence of micritic envelopes, bioturbation, biofouling, and cement infill on the age.

Keywords: *Petaloconchus varians; Tetraclita stalactifera;* Mytilida; paleo-sea level; radiocarbon dating; AMS dating; Holocene highstand.

1. Introduction

Vermetid gastropod bioconstructions have been used as paleo-sea level indicators along the Brazilian coast since the seminal work of Van Andel and Laborel (1964). From the mid 20th century onward, hundreds of dated samples have been used to determine paleo-sea levels and build up Mid- to Late-Holocene relative sea-level curves (e.g. Martin et al., 2003; Angulo et al., 2006). In particular, bioconstructions of *Petaloconchus varians* (d'Orbigny 1841), the most common species of vermetid in Brazil, have been considered one of the best Holocene sea-level indicators (e.g. Angulo et al., 2006; Angulo and Souza, 2014; Toniolo et al., 2020). Most of the age determinations from this species have been performed using conventional ^{14}C dating, which demands large (25-30 g) samples (e.g. see compilations by Martin et al. 2003 and Angulo et al. 2006). More recently, smaller vermetid samples (10-25 mg) have been dated using the Accelerator Mass Spectrometry (AMS) method (e.g. Toniolo et al. 2020, Angulo et al. 2022a, 2022c). Furthermore, vermetid bioconstructions may also contain the remains of several other species that precipitate carbonate shells, including mollusks and barnacles (Angulo, 1992, 1993; Angulo and Souza, 2014; Angulo et al., 2022a). Therefore, this work explores the potential for dating shells of different species within vermetid bioconstruction remains to identify whether they are synchronous or diachronous with *P. varians*. The main importance of establishing the relationship of ages lies in the fact that it could help to reveal the direction or tendency of past changes in sea level. For example, if species that live on a lower or a higher fringe are superposed on the vermetid fringe, this would indicate that sea level was raising or lowering, respectively. To test this hypothesis, we chose four vermetid bioconstruction remains previously dated using bulk samples (Angulo, 1989, 1992; Angulo et al., 2002, 2022a), to have shells of different species dated individually by ^{14}C AMS. This hypothesis test assumes that the ^{14}C dating results obtained from the different species are reliable indicators of the life span of each building animal. In view of this, a parallel objective of this work is to analyze the reliability of the ages

obtained from each species, based on aspects such as their purity, alteration and neomorphism.

Vermetid bioconstructions

Vermetid bioconstruction remains are widely dispersed along the Brazilian coast. They occur, at least, from Cristovão, Rio Grande do Norte state (4° 55’ S, Bezerra et al., 2003) to Santa Marta Cape, Santa Catarina state (28° 36’ S, Angulo et al., 1999). They are found on the mainland and on several oceanic islands such as São Pedro & São Paulo (0° 55’ N, Angulo et al., 2013a), Rocas Atoll (3° 52’ S, Angulo et al., 2022c), Fernando de Noronha (3° 49-52’ S, Angulo et al., 2013b), Abrolhos (17° 58’ S, Angulo et al., 2022b) and Trindade (20° 30’ S, Angulo et al., 2013b) (Fig. 1). Therefore, they can provide useful data to construct or refine Mid- to Late-Holocene sea level curves along the western Atlantic Ocean coast.

Two species are the main vermetid reef builders along Brazilian coasts: *P. varians* and *Dendropoma irregulare* (d’Orbigny 1842) (Laborel, 1969, 1979, 1986; Spotorno-Oliveira et al., 2012). Subfossil bioconstructions, as well as bioconstructions with living vermetids, occur fixed to rock substratum. *P. varians* lives at the upper limit of the infra-littoral zone (sensu Peres and Picard, 1964) or the lower midlittoral fringe (sensu Stephenson and Stephenson, 1949) (Laborel and Kempf, 1966; Kempf and Laborel, 1968; Laborel 1968, 1969, 1977, 1979, 1986). Its biological zone is not strictly horizontal and the altitude varies according to wave exposure and tidal range (Laborel and Kempf, 1966; Kempf and Laborel, 1968; Laborel 1969, 1979, 1986). In biological zonation, *P. varians* bioconstructions are associated with calcareous algae. According to Laborel (1979), they are located above the red algae fringe and below the *Tetraclita stalactifera* (Lamarck, 1818) fringe. The upper part of the *P. varians* biological zone coincides with the lower part of that of *T. stalactifera* and the two species can coexist in life in the same bioconstruction (Laborel, 1979; Angulo et al., 2022a). The ecological conditions of these two species are similar to those observed in the polychaete *Phragmatopoma sp.* and in the bivalves *Leiosolenus bisulcatus* (A. d'Orbigny, 1853), *Petricola bicolor* G. B. Sowerby II, 1854, and *Petricola stellae* Narchi, 1975 (Narchi, 1974, 1975; Angulo and Souza, 2014; Pardal et al., 2023).

Colonial vermetids, which built reefs, are widely dispersed in tropical and subtropical waters along high-energy rocky coasts (Laborel, 1986). Donnarumma et al. (2021), studying Mediterranean reefs of living *Dendropoma* vermetids, detected a well-defined zonation pattern, with a gradual decrease in structural complexity (e.g. indentation degree) from the outer edge, facing the open-sea, to the inner edge. Such structural complexity zonation reflects underlying environmental gradients and plays a crucial role in the distribution of associated benthic communities (Picone and Chemello, 2023).

On the Brazilian mainland coast, the southern limit of occurrence of living colonies is between Cabo Frio (22° 54’ S, Laborel, 1986) and the south of the Rio de Janeiro state (23° 05’ S, Spotorno-Olveira et al., 2012, Breves et al., 2017, Toniolo et al., 2020), over 5° north of the southern limit of occurrence of bioconstruction remains, at Santa Marta Cape (Angulo et al., 1999). The presence of these bioconstruction remains south of the current range of living vermetids is probably related to the occurrence of warmer waters during the Holocene climatic optimum (Laborel, 1977, 1979, 1986; Angulo et al., 1999) or in specific time intervals of the Mid- and Late-Holocene (Toniolo et al., 2020). In the

southern Brazilian region, vermetid bioconstruction remains were reported from Cardoso Island (25° 11’ S, Angulo et al., 2006) to Santa Marta Cape (Fig. 1). They occur attached to igneous and metamorphic rocks exposed to breaking wave action.

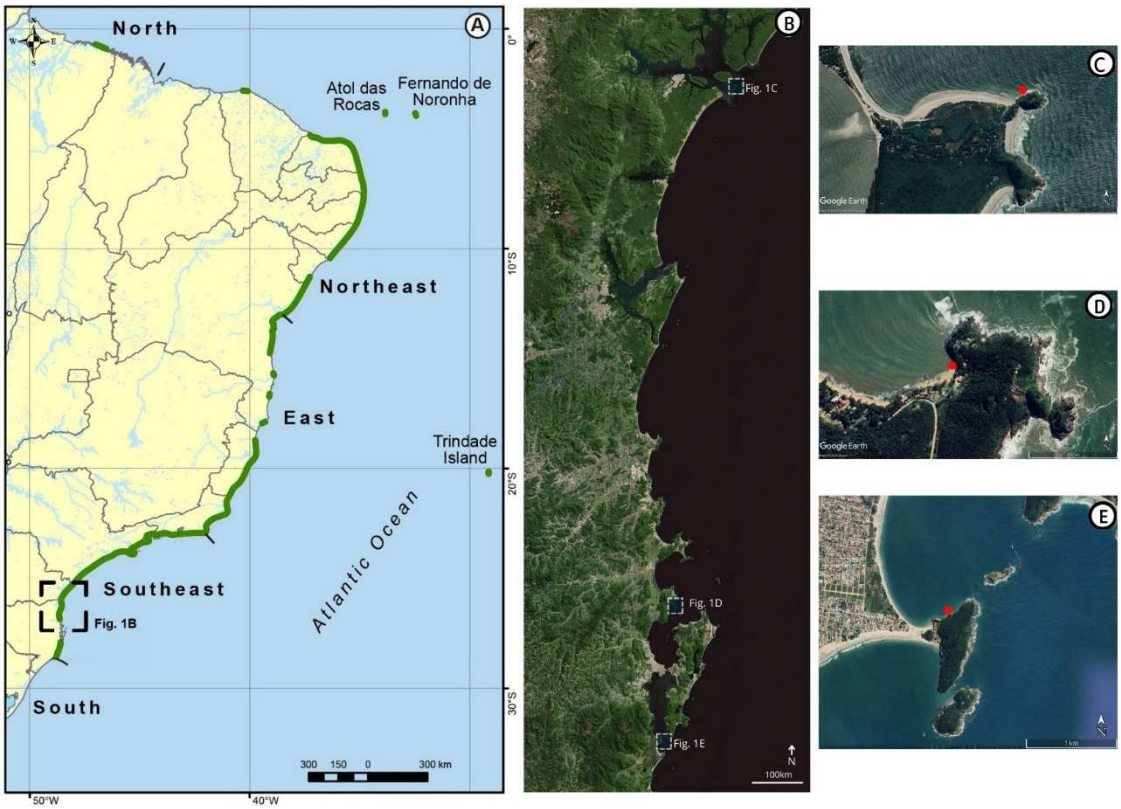

Fig. 1: Distribution of vermetidae bioconstruction remains on the mainland and oceanic island coasts of Brazil (A, green line), and locations where the vermetid bioconstruction samples were obtained for this work (B): Ilha do Mel (C), Armação do Itapocoroi (D), and Ponta do Papagaio (E).

2. Regional setting and study area

From a coastal physiography standpoint, the study area can be divided into two sectors (Giannini et al., 2007, 2009, Hesp et al., 2009), both with inland high relief, supported by crystalline rocks (Dominguez, 2009). In the northern sector, north of latitude 26° 24’ S, the coastline lies between the Serra do Mar, a mountain range with an altitude of over 1900 m, and the Santos Basin. The Serra do Mar delimits a series of large Quaternary estuaries (tens to hundreds of km²), such as the bays of São Francisco, Laranjeiras, Paranaguá and Guaratuba (Angulo et al., 2009, 2016, 2018; Giannini et al., 2009; Hesp et al., 2009). In the southern sector, the coastline lies between the Serra do Taboleiro, reaching up to 1300 m, and the Florianópolis Paleogene submerged structural high, which separates the Santos and Pelotas basins. This sector has a narrower and steeper inner shelf and a more restricted coastal plain (Giannini et al., 2007), and is also more rugged, with headlands, rocky shores, pocket beaches and small embayments, including log-spiral ones (Hesp et al., 2009).

The coastline is characterized by the alternation between quartzose sandy beaches and rocky headlands. The headlands are formed of gneisses and migmatites of the Lower Proterozoic Coastal Complex, which are intruded by a Lower Cretaceous basaltic dike system related to the opening of the South Atlantic Ocean (Mineropar, 1989; Wildner et al., 2014).

The regional climate is mesothermic wet subtropical, without a dry season and with a warm summer (Monteiro and Furtado, 1995). Cyclonic winds from E and NE predominate during spring-summer and winds generated by cold fronts from S and SW predominate during autumn-winter (Mendes and Giannini, 2015).

The tide in the region is microtidal and semi diurnal with diurnal inequalities (DHN, 2023). The mean tidal range is 1.5 m at Ilha do Mel (Marone and Jamiyanaa, 1997) and decreases to the south, reaching 0.6 m at Imbituba Port, located 35 km south from Ponta do Papagaio (CHM, 2020, Fig. 1).

Offshore, the seasonal mean wave heights range from 1.7-1.9 m with mean periods of 7.7-7.8 s in the spring-summer to 2.0-2.2 m with period of 8.9-8.7 s in the autumn-winter (Pianca et al., 2010). The main wave directions are from NE and E during spring-summer and from S and SE during the autumn-winter (Pianca et al., 2010).

Study area

The study sites are Ponta das Conchas, at Ilha do Mel (25º 32’ 19’’ S, 48° 17’ 30’’ W), Praia da Armação do Itapocoroi, in Penha (26º 46’ 53’’ S, 48° 36’ 08’’ W), and Ponta do Papagaio, in Palhoça (27º 50 43’’ S, 48° 24’ 45’’ W), on the Southern Brazilian coast (Fig. 1). At these sites, bulk samples of vermetid bioconstruction remains were dated in previous works (Angulo, 1989, 1992; Angulo et al., 2022a). These samples give ages from 1045 ± 75 aBP (Angulo, 1989) to 3860 ± 80 aBP (Angulo et al., 2022a) and indicate sea levels between 1.5 ± 0.3 m (Angulo et al., 2022a) and 2.9 ± 0.5 m (Angulo, 1992; Angulo et al., 2022a) above present (Table 1).

The vermetid bioconstructions from Ponta das Conchas occur on a rocky coast moderately exposed to waves, under a boulder approximately 3 m in diameter. In the 1980s, the lower limit of terrestrial plants was near the vermetid bioconstruction remains, which were penetrated by some roots (Angulo, 1993). In 2025, that limit had lowered, surrounding the boulder, and vermetid remains were no longer visible. This change in plant distribution was favored by sand deposition in front of the rocky coast, which reduced wave action. The sand supply also favored the growth of *Phragmatopoma caudata* bioconstructions. The top of these bioconstructions was considered equivalent to the top of the vermetid bioconstructions and used to determine the paleo-sea level, since bioconstructions with living vermetids are missing from this region (Angulo, 1993).

The vermetid bioconstructions remains at Praia da Armação de Itapocoroi were 40 cm thick and, in the 1980s, covered by a thin sand cover, being exposed by erosion generated by a small pedestrian trail (Angulo, 1989). In 2024, the sand was completely eroded and only gravels constituted by vermetid bioconstructions were found on the beach.

The vermetid bioconstruction remains at Ponta do Papagaio occur under granitic boulders, where they remained relatively protected from freshwater dissolution and wave action (Angulo et al. 2022a).

196

197 Table 1: Paleo-sea levels and conventional radiocarbon and calibrated ages (SHCal20 curve) before present (BP) of bulk vermetid bioconstructions, published
198 in former works, and of different species associated to vermetid bioconstructions dated in the present work.

Sample ID	Location	Material	Lab. code	Radiocarbon age (aBP)	Calibrated age (aBP)	Paleo-sea level (m)
PCIM	Ponta das Conchas, Ilha do Mel	Bulk	GSC-5255[(1)]	3500 ± 60[(1)]	3897-3499	2.9 ± 0.3[(1)]
		Pv[(a)]	Beta-618167	5890 ± 30	6781-6556	
		Ts[(a)]	Beta-618168	6020 ± 30	6941-6684	
		My	Beta-618169	4600 ± 30	5441-5051	
		Oy[(b)]	Beta-618170	5960 ± 30	6852-6659	
PA	Praia da Armação do Itapocorói	Bulk	GX-14061[(2)]	1045 ± 75[(2)]	1057-741	2.6 ± 0.3 [(3)]
		Pv[(a)]	Beta-618171	1500 ± 30	1405-1302	
		Pv[(c)]	Beta-618172	1460 ± 30	1363-1282	
		Ts[(a)]	Beta-618173	1490 ± 30	1403-1298	
Pnh2	Ponta do Papagaio	Bulk	CEN-1005[(4)]	2310 ± 70[(4)]	2489-2063	1.5 ± 0.3[(4)]
		Pv	Beta-618174	2510 ± 30	2719-2367	
		Ts	Beta-618175	2550 ± 30	2741-2437	
Pnh5	Ponta do Papagaio	Bulk	CEN-1008[(4)]	3860 ± 80[(4)]	4501-3936	2.4 ± 0.3[(4)]
		Pv[(a)]	Beta-618176	5040 ± 30	5894-5604	
		Ts[(a)]	Beta-618177	5340 ± 30	6260-5943	
		My[(d)]	Beta-618178	4740 ± 30	5575-5321	

199 Notes: (aBP) years before present; (GSC) Geological Survey of Canada, (GX) Kruger Enterprises Inc. Geochron Laboratories Division, (CEN) Radiocarbon Laboratory of the
200 Center for Nuclear Energy in Agriculture (CENA), (Beta) Beta Analytic.; (Bulk) Bulk vermetid bioconstruction; (*Pv*) *P. varians;* (*Ts*) *T. stalactifera;* (My) Mytilida *L.* af. *bisulcatus*;
201 (Oy) Oyster, (a) from the bioconstruction bottom, (b) small shell fixed inside the *T. stalactifera* shell, (c) from the bioconstruction top, (d) for complete the mass, the sample
202 was composed by one shell plus shell fragments of three other specimens. References: (1) Angulo, 1992; Angulo et al., 2002, (2) Angulo, 1989, (3) Angulo et al., 2006, (4)
203 Angulo et al., 2022a. The error margin of samples PCIM and PA were adjusted according to Angulo et al. (2022a).

3. Methods

Bioconstruction samples ranging in width from cm to dm and thickness in cm were collected in the field at the four study sites. In the laboratory, taxa were identified and their associations described across the thickness of the bioconstruction, that is, between the surface adhered to the rock (here designated as the basal surface) and the opposite (exposed or apical) surface.

Whole shells or pieces of shell from different species of the four previously dated vermetid bioconstructions were separately extracted (Table 1). Selected aliquots of this material, showing no evidence of cementation under a 10X hand lens, were dated by ^{14}C AMS at Beta Analytic Inc., Miami, USA. Conventional ^{14}C ages were calibrated using CALIB version 8.2 (Stuiver and Reimer, 1993) and the and the SHCal20 Southern Hemisphere calibration curve (Hogg et al., 2020).

Aliquots (~2-10 cm^3) were extracted from the same bioconstructions samples, for thin section microscopy analysis. They were initially examined using a reflected light stereoscopic magnifying glass up to 60x (Carl Zeiss, model Stemi SV.11). Digital images were acquired by a coupled camera (Leica MC170HD) with a multifocal acquisition device. Each sample was then vacuum-impregnated using a liquid mixture of Epoxy resin and blue dye. The aim was to allow differentiation between the original (colored) pores and the artificial (colorless) ones subsequently induced by the thin sections preparation. These sections, ~30 μm thick, were obtained transversally to the bioconstruction thickness.

The descriptions of the four thin sections were completed with a polarized light microscope (Carl Zeiss, model Axioplan) with maximum magnification of 1000x, coupled with Leica Application Suite (LAS) software and a Leica MC170HD photographic camera.

The analysis of each thin section under the optical microscope included: 1. recognition and percentage estimation of six major components: biogenic growth framework, extraclastic (terrigenous) silty sand fill, intraclastic silty sand fill, syn- or post-depositional clayey matrix, cement and original pores; 2. identification and percentage estimation of mineralogical components of the terrigenous fraction; 3. characterization of the terrigenous fraction in terms of texture (modal grain size, on the Wentworth 1922 scale, and estimation of quartz roundness according to the Powers 1953 graphic scale) and fabric (e.g., packing, spatial segregation and grading); 4. identification and percentage estimation of types of intraclast; 5. characterization of the intraclastic fraction in terms of texture (modal grain size) and fabric; 6. description of the mineralogy, texture and fabric of the matrix and cement; 7. characterization of the macro- and meso-pores (larger than clay size, according to Pittman, 1979) regarding shape and fabric based on Choquette and Pray (1970); and 8. classification of the depositional fabric of the bioconstruction as a whole.

To describe the constituent parts of the main bioconstructor organisms, the nomenclature used by d'Orbigny (1841), Laborel (1986), Savazzi (1996) and Scuderi (2012) was adopted, in the case of vermetids, and Tsang et al. (2015), in the case of barnacles.

In the description of the thin section, emphasis was placed on the relationships between vermetids and barnacles *in situ* and with other components in general. Particular attention was given to the possible presence of features indicative of neomorphism of their carbonate, or other post-depositional modifications, such as surface alteration, encrustation or breakage, that could have influenced in some way the dating results.

4. Results

4.1. Ages and description of samples

The conventional and calibrated ^{14}C ages of the shell samples of different species from the studied sites are presented at Table 1. A description of the bioconstruction components follows, organized by collection site.

Ponta das Conchas, Ilha do Mel

The vermetid bioconstruction remains from Ponta das Conchas, Ilha do Mel, are approximately 11 cm thick. Barnacles were observed in the apical, middle, and basal zones, through its thickness. The bioconstruction is constituted by *P. varians* tubes, *T. stalactifera* shells, and borings attributed to Mytilida cf. *Gastrochaenolites* isp., sometimes with the *L.* af. *bisulcatus* shells in life position inside. In addition, a cemented chela of a crustacean and a *Bostrycapulus aculeatus* (Gmelin, 1791) shell, were identified at the basal surface; and oysters were found on the exposed surface of vermetid bioconstruction, thus totaling seven identified taxa (Table 2, Figs. 2A and 2B). The external surface of the vermetid bioconstruction presented typical signals of carbonate dissolution similar to lapiés (Fig. 2A). The vermetids were superposed on the *T. stalactifera* shells and, sometimes, the vermetids tubes penetrated the barnacle by the upper opening, indicating that the *T. stalactifera* specimens were dead when the vermetids grew (Fig. 2B).

Fig. 2: Apical (A, B and C) and basal (D and E) surface views of Ponta das Conchas bioconstruction of *Petaloconchus varians* with: *Tetraclita stalactifera* (t)*;* boreholes of Mytilida (b). Notice the vermetid tube growing inside the upper opening of a *T. stalactifera* shell (arrow).

The age of different species from the Ponta das Conchas sample ranged from 6,941-6,684 cal aBP (*T. stalactifera*) to 5,441-5,051 cal aBP (Mytilida) (Table 1). The age of the different species correspond to the expected life sequence inferred from the observation of the samples (Fig. 2). First, the *T. stalactifera* fixed on the naked rock at 6,941-6,684 ^{14}C cal aBP; subsequently, the *T. stalactifera* died and a small oyster fixed inside the barnacle shell at 6,852-6,659 ^{14}C cal aBP. After that – 6,781-6,556^{14}C cal aBP – *P. varians* grew over the barnacles and oyster. Finally, the lithophagus Mytilida bored the bioconstruction at 5,441-5,051 ^{14}C cal aBP (Table 1).

At Ponta das Conchas, it was observed that the top of the *P. caudata* bioconstruction corresponds to the lower limit of the fringe of *T. stalactifera*, which agrees with the former paleo-sea level reconstruction (Angulo, 1989 and 1992; Angulo et al., 2002, 2006 and 2022a).

Praia da Armação de Itapocoroi

The bioconstruction remains from Praia da Armação de Itapocoroi presented the vermetid tubes arranged in three overlapping layers approximately 3 cm thick, totaling 9 cm between basal and apical surfaces (Fig. 3A). At the basal zone, the tubes were spiral in shape and, from the middle to the apical zone, they were almost linear and vertical (Fig. 3). This bioconstruction is constituted by *P. varians* tubes, *T. stalactifera* parietal plates, borings of Mytilida (*Gastrochaenolites* isp.), and shells of venerid bivalves, sometimes with articulated shells of the *P.* aff*. bicolor* inside. Furthermore, oysters occur in cavities amid the vermetid bioconstruction. A total of 11 taxa associated with the vermetid bioconstructions were identified (Table 2, Figs. 3A and 3B).

Table 2: Invertebrate diversity associated with vermetid bioconstructions remains.

Taxa	**Sample** (Zone)*			
	PCIM (IR; CV)	**PA** (OR)	**PNH2** (CV)	**PNH5** (IR)
Arthropoda				
Crustacea				
Balanomorpha				
Tetraclitidae				
Tetraclita stalactifera (Lamarck, 1818)	X	X	X	X
Decapoda sp.1 **	X			
Equinodermata				
Echinoidea sp. 1 ***			X	
Mollusca				
Polyplacophora				
sp. 1			X	
Calloplax af. *janeirensis* (Gray, 1828) ****			X	
Bivalvia				
Ostreida				
Ostreidae	X	X	X	
Crassostrea sp. 1			X	
Ostrea sp.1			X	X
Mytilida				
Mytilidae				
Leiosolenus af. *bisulcatus* (d'Orbigny, 1853)	X	X	X	X
Mytilaster solisianus (A. d'Orbigny, 1846)		X	X	X
Modiolus sp. 1			X	
sp. 1		X	X	
sp. 2			X	
Venerida				
Veneridae				
Petricola af. *bicolor* Sowerby II, 1854		X	X	X
Chamidae			X	
Chama af. *congregata* Conrad, 1833				X
Myida				
Corbulidae				
Corbula sp. 1			X	
Gastropoda				

Lottiidae				
Lottia subrugosa (A. d'Orbigny, 1841)		X	X	X
Littorinimorpha				
sp. 1		X		
sp. 2			X	
Calyptraeidae				
Bostrycapulus aculeatus (Gmelin, 1791)	X		X	
Ergaea walshi (Reeve, 1859)			X	
Vermetidae				
Petaloconchus varians (d'Orbigny 1841)	X	X	X	X
Littorinidae				
Littoraria flava (King, 1832)			X	
Fissurela itapema (Ihering, 1927)			X	
Diadora af. *meta* (Ihering, 1927)		X		
Anellida				
Sabellida				
Serpulidae	X	X	X	X
Total (n)	**7**	**11**	**23**	**9**

Notes: * Donnarumma et al. (2021); Picone and Chemello (2023) references; ** chela of a crustacean; *** spine; **** intermediate valve.

The age of different species ranged from 1,405-1,302 cal aBP to 1,363-1,282 cal aBP, which correspond to the basal and apical generations of *P. varians,* respectively (Fig.3A). The *T. stalactifera* shell presented an age of 1,403-1,298 ^{14}C cal aBP, within the age uncertainty of the basal generation of *P. varians*.

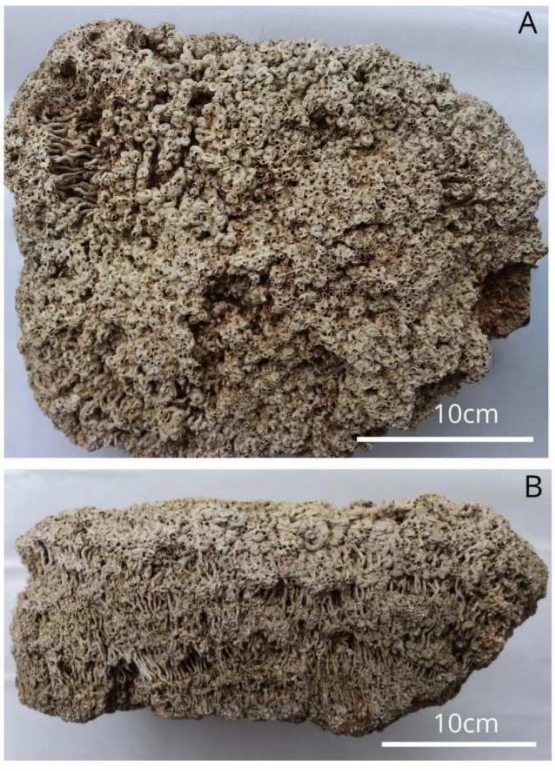

Fig. 3: Apical (A) and lateral (B) surface sample views of the Praia da Armação vermetid bioconstruction remains.

Ponta do Papagaio 2 and 5

The vermetid bioconstructions remains corresponding to samples Pnh2 and Pnh5 from Ponta do Papagaio consist of *P. varians* tubes approximately 6 cm thick, with *T. stalactifera* and Mytilida borings (*Gastrochaenolites* isp.) and Veneridae, sometimes with shells of *P.* aff*. Bicolor, L.* aff. *bisulcatus* (in sample Pnh5), and *M. solisianus* in life position inside.

At sample Pnh2, cemented shells of oysters and three gastropod species (*L. subrugosa*, *E. walshi*, and *B. aculeatus*) were identified in the middle and apical zones of the bioconstruction. A greater abundance of barnacles was observed in the middle and basal zones. Within the barnacle assemblage, serpulid Polychaeta tubes, oyster and *Littoraria flava* shells, and *P. varians* tubes were recognized, primarily distributed in the basal and middle zones. A total of 23 taxa were identified (Table 2, Figs. 4A and 4B).

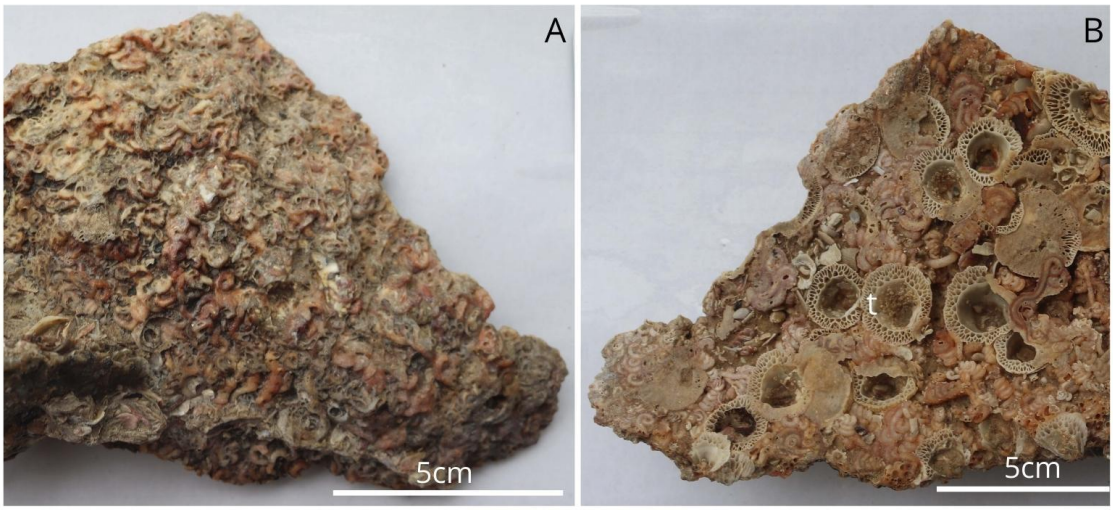

Fig. 4: Apical (A) and basal (B) surface views of Ponta do Papagaio vermetid bioconstruction, sample Pnh2, with *Tetraclita stalactifera* (t) shells.

At sample Pnh5, the barnacles were observed in the apical and middle zones of the bioconstruction, inside the borings attributed to Mytilida, and serpulid Polychaeta tubes. Cemented *L. subrugosa* shells were recognized at the basal surface. A total of nine taxa were identified (Table 2, Figs. 5A and 5B).

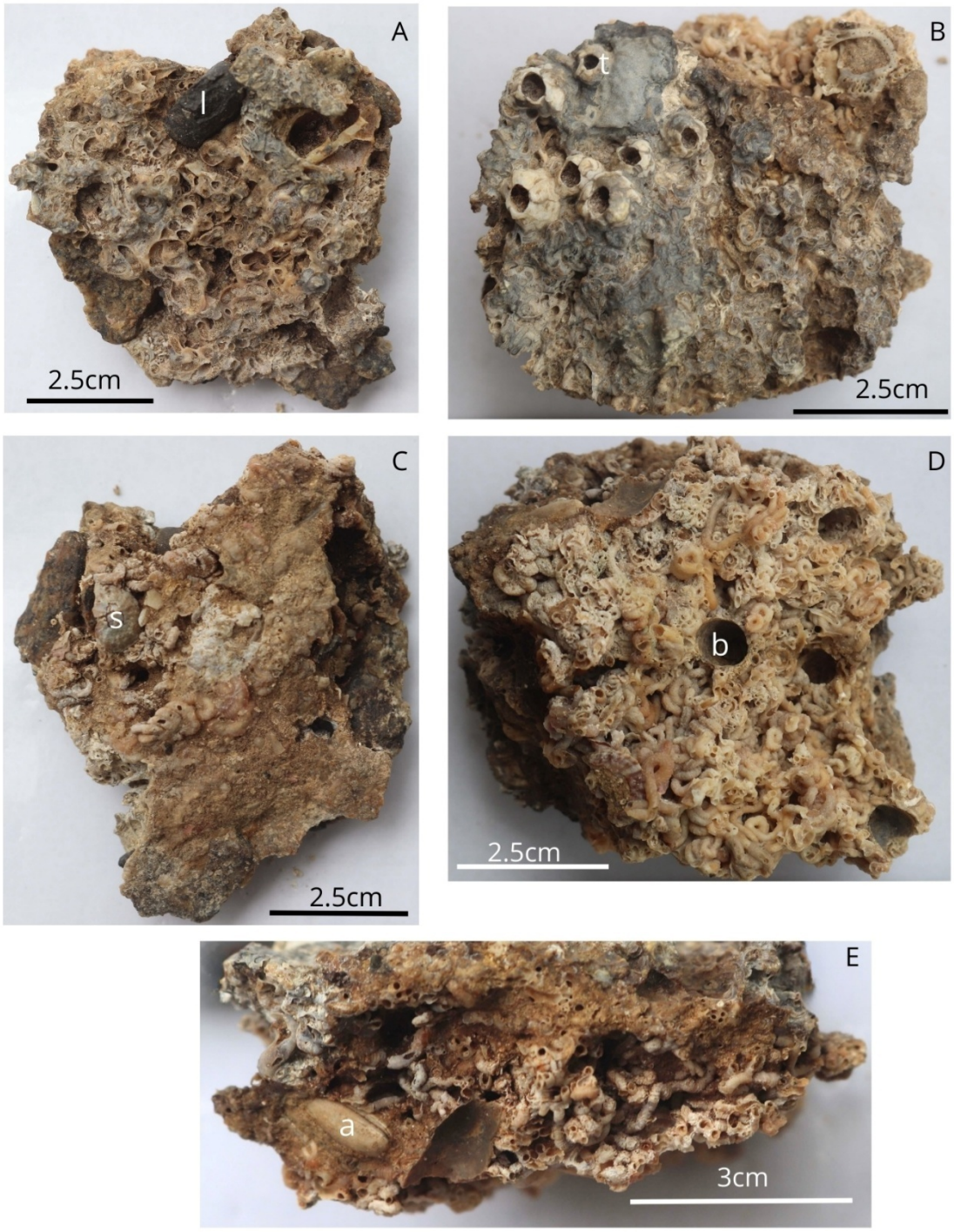

Fig. 5: Apical (A and B), basal (C and D), and lateral (E) surface views of Ponta do Papagaio vermetid bioconstruction, sample Pnh5, with: l. lithic gravels; t. *Tetraclita stalactifera* shells on the bioconstruction surface; b. Mytilida boring (*Gastrochaenolites* isp.); a. articulated shells of *Leiosolenus* aff. *Bisulcatus*, in living position; s. *Lottia subrugosa* shell.

The ages of *P. varians* and *T. stalactifera* shells from sample Pnh2 were similar – 2,719-2,367 ^{14}C cal aBP and 2,741-2,437 ^{14}C cal aBP, respectively. In contrast, the ages of

different species from the sample Pnh5 ranged from 6,260-5,943 ^{14}C cal aBP to 5,575-5,321 ^{14}C cal aBP.

4.2. Optical microscopy analysis

When observed under the stereoscopic magnifying glass (Fig. 6), *P. varians*, *T. stalactifera* and *L.* af. *bisulcatus* presented homogeneous color, both internally and externally. Under the magnifying glass and microscope (Figs. 7 to 10), *P. varians* showed four main shapes: spiral or concentric; subcircular to oval (Figs 6A and 6B); similar to a cloverleaf or a pair of symmetrical cloverleaves (Fig. 9A); and similar to a bean or dumbbell (Fig. 7A). The internal diameter of the tubes varied around 1.2 mm, and the wall thickness around 0.2 mm (Figs. 6 and 7). External ornamentation was typical of the gastropod species (Fig. 6B), in the form of either transverse striations, corresponding to the tube growth lines, or longitudinal ridges. In cross-section of the tube, the longitudinal lines appeared as subtle (Figs. 9A and 10A) to sharp (Fig. 8D) undulations on the outer surface of the tube.

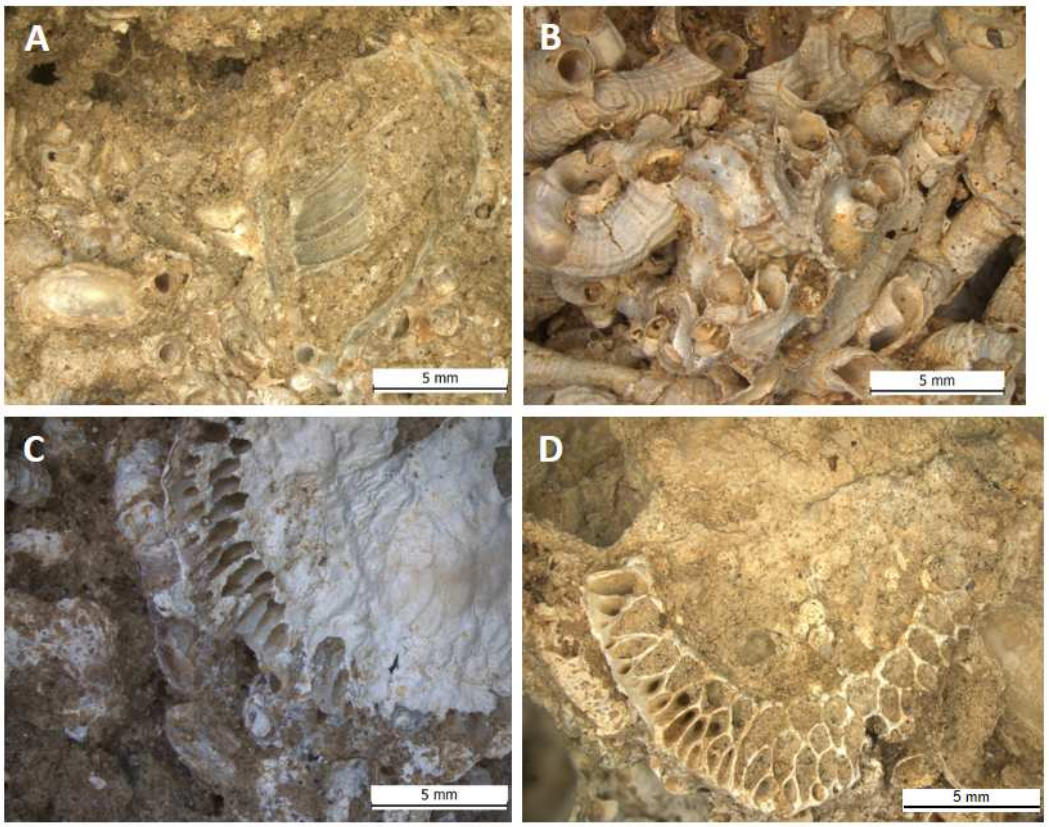

Fig. 6: General appearance of the studied bioconstruction samples under reflected light stereomicroscope: A. Vermetids (v) and Mytilida (M) shell filled with micrite and sand grains (c) in sample PCIM. B. PA sample with vermetids (v), bryozoan encrustation (b) and clastic filling (c). C. Flat basal surface of sample Pnh2, with barnacle (t) surrounded by vermetids. D. Sample Pnh5 exhibiting barnacle (t) overgrown by vermetids (v). Note the barnacle parietal tubes (pt) in C and D.

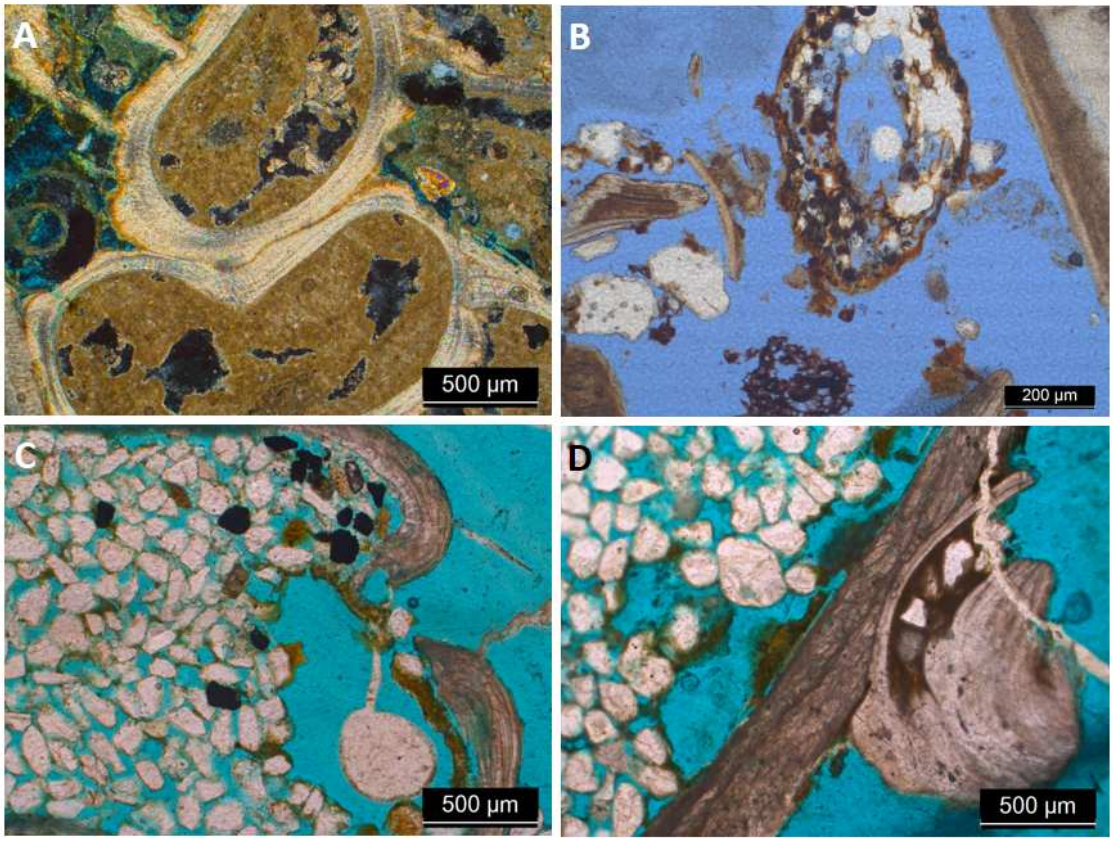

Fig. 7: Components of the framework under polarized transmitted light microscopy: A. Vermetids (v) and smaller gastropod (g) in sample PCIM. Note the vermetid chambers with brown outer envelope (e) and filled by micrite (m) containing elongated pores. B. Plant remains (p) in sample PA, including probable rootlet. C. *Leiosolenus* af. *bisulcatus* valves in sample Pnh2. Note the filling with terrigenous clasts (q), including opaque heavy minerals, and clay-ferruginous cement (f). D. Vermetid (v) attached to a barnacle (t) in sample Pnh5. Note the filling with terrigenous clasts (q) and micrite (m), including inside the vermetid. Crossed polarizers in A and parallel polarizers in B, C and D.

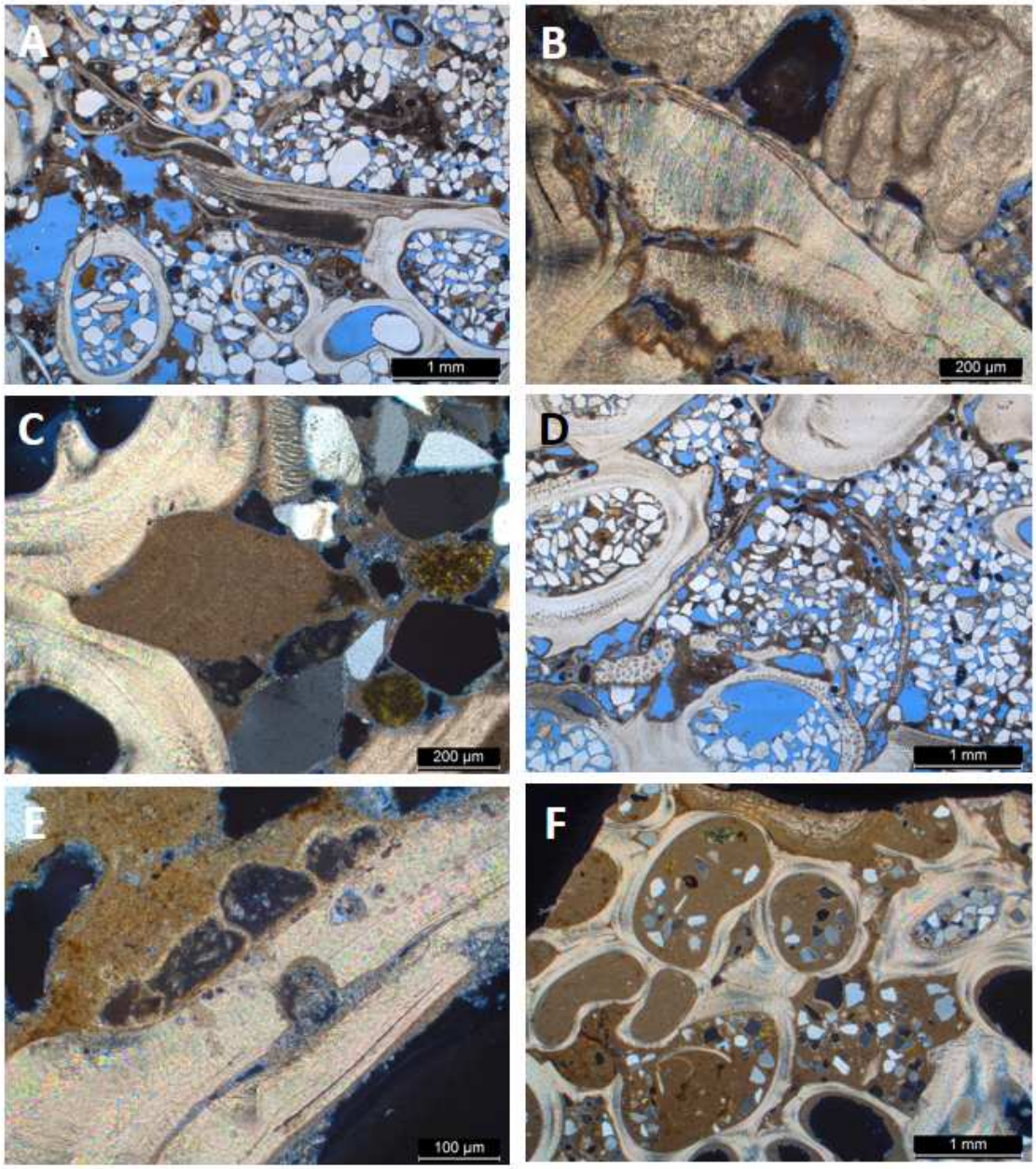

Fig. 8: Associations between bioconstructor organisms in sample Pnh5, under polarized transmitted light microscope: A, B. Vermetid (v) – barnacle (t). C: Vermetid (v) – red algae (r) . D. Vermetid (v) – bivalve (supposedly Mytilida, M). E. Vermetid (v) – encrusting foraminifera (ef). F. Microbial mat (cb) on top of the vermetid (v) bioconstruction. Note the intense filling of the chambers by terrigenous grains (q) and micrite (m). Parallel polarizers in A and D, and crossed polarizers in B, C, E and F.

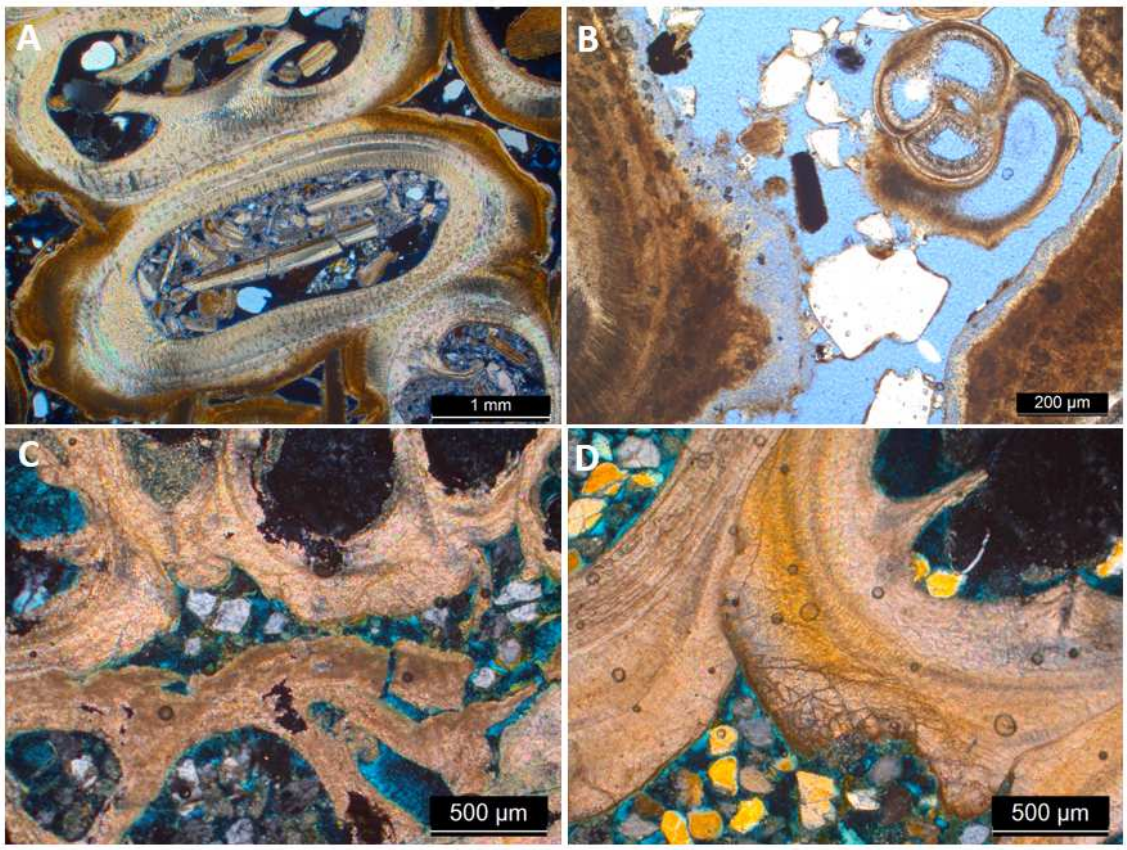

Fig. 9: Post-depositional modifications in the vermetid bioconstruction framework (v): A. Dark brown outer border, with the appearance of a micritic envelope (e) (sample PA). B. External anisopaque coating, constituted of thin carbonate, attributed to encrustation by a bryozoan (b) (sample PA). C. Chemical alteration and dismantling at the top of the bioconstruction, overlapped by a new horizon of unaltered chambers, suggestive of a pause in colony growth (sample Pnh2). D. Dark, cracked outer border (e) (sample Pnh2). Note the partial filing of the pores by bioclasts (c) and terrigenous material (q). Crossed polarizers in A, C and D, and parallel polarizers in B.

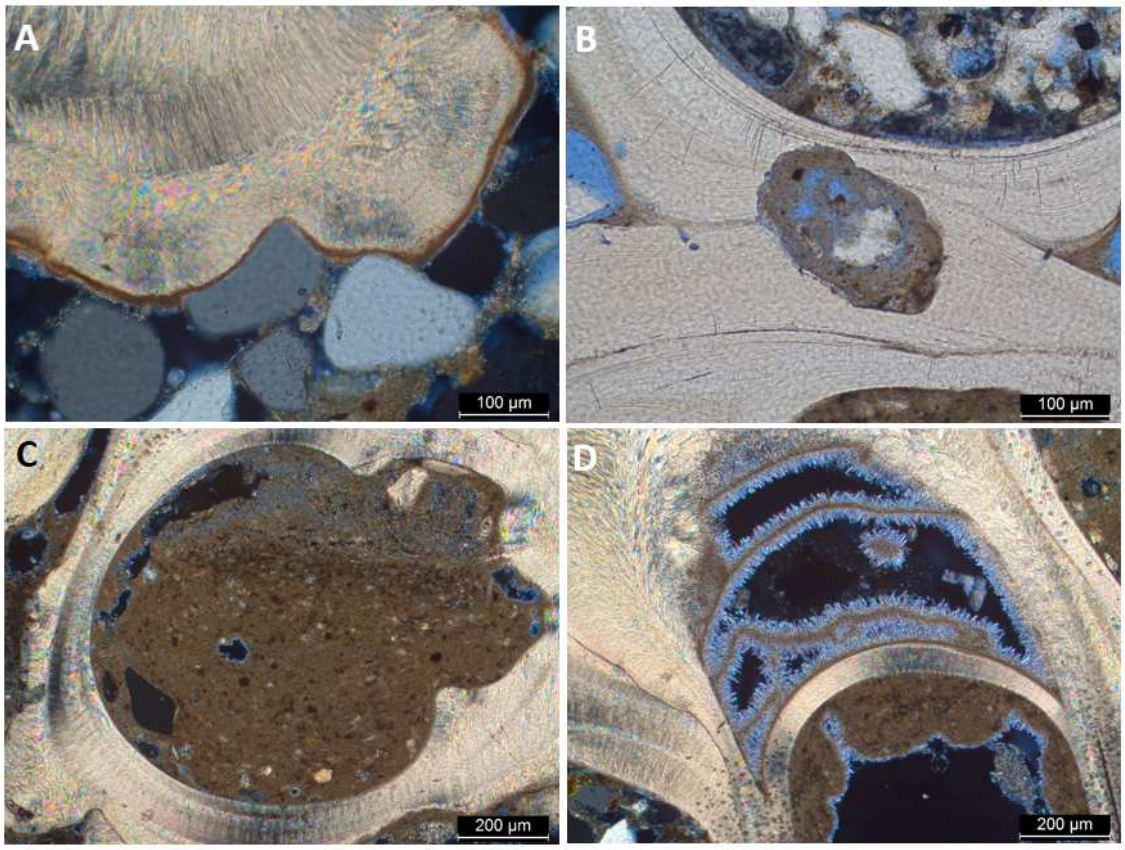

Fig. 10: Post-depositional modifications of the vermetid framework (v) in sample Pnh5: A. Dark brown outer border, with the appearance of a micritic envelope (e), showing adhered quartz grains (q). B. Bioperforation crossing the contact between two adjacent chamber walls, partially filled with micrite. C. Filling of the chamber by two generations of micrite, in a geopetal pattern. D. Partial filling of the chambers by anisopachous pendulous micrite (m) and isopachous fringe of microspar (ms). Crossed polarizers in A, C and D, and parallel polarizers in B.

In *T. stalactifera*, the parietal tubes exhibited a polygonal shape in cross-section, with a major axis of 0.2 to 1.0 mm (Fig. 6D), or an elongated arch, up to approximately 2 mm long (Fig. 6C). The wall thickness (septum) was similar to that of the vermetid, but the shell edges (inner and outer lamella) could reach several millimeters thick. The carbonate coloration is slightly darker than that of the vermetid (Figs. 7D, 8A and 8B) and with the occasional presence, inside, of elongated pockets (Fig. 8A) and serrated or parabolic shapes (Fig. 8B) that are even darker, almost black.

The flat surface by which the shells were attached to the rocky shore appeared better developed or evident in the barnacle than in the vermetid (Figs. 6C and 6D). A concentric relationship between the two, with *T. stalactifera* serving as the growth nucleus of *P. varians*, was sometimes noticeable (Figs. 6C and 6D).

The summary of the thin section descriptions is given in Table 3. The depositional fabric of the four samples was carbonatic growth framework, with partial filling dominated either by micrite (PCIM) or by extraclastic (terrigenous) sand-silt (other samples). Despite this, the growth framework was only the major textural component of the

encrustations in one sample (Pnh5). In the others, the dominant component was either micrite (PCIM) or pores (PA and Pnh2).

411

412 Table 3: Summary of carbonate bioconstructions petrographic analysis. TR = trace amount (<<1%). HM = heavy mineral.

Component		Sample			
		PCIM	**PA**	**PNH2**	**PNH5**
Growth framework	**Proportion (%)**	**25**	**25**	**35**	**35**
	Composition	*P. varians* (100), Mytilida (TR), other gastropode (TR)	*P. varians* (96), bryozoan (2), traces of vegetables, including rootlets (2)	*P. varians* (65), *T. stalactifera* (30), Mytilida (5)	*P. varians* (75), *T. stalactifera* (15), red algae (4), Mytilida (4), other gastropode (1), encrusting foraminífera (1)
Extraclastic (terrigenous) silty-sand fill	**Proportion (%)**	**5**	**10**	**10**	**20**
	Composition	Quartz (95), feldspar (5), opaque HM (TR)	Quartz (90), lithic fragment (6), composite grain rich in opaque HM (3), feldspar (1), HM (TR)	Quartz (95), feldspar (3), opaque HM (2), transparent HM (TR)	Quartz (95), feldspar (2), chert (2), opaque HM (1), transparent HM, e.g. tourmaline, zircon (TR)
	Texture	Coarse silt to coarse sand sub-angular to well-rounded grains	Very fine to very coarse sand sub-angular grains	Coarse silt to median sand angular to sub-rounded grains	Well sorted very fine to fine sand angular to sub-rounded grains
	Fabric	Larger loose grains filling the tubes and smaller grains in the middle of the matrix	Preferential occurrence between tubes	As filling, in most bioconstruction pores, locally appearing normal gradation	As intra and inter-tube filling; partial intratube filing occasionally in geopetal pattern
Intraclastic silty-sand fill	**Proportion (%)**	**1**	**7**	**2**	**5**
	Composition	Elongated and isolated ellipsoidal (rings) fragments of vermetidae (70), phyllossilicate grains (20), ferruginous grains (10)	Elongated to subequidimensional vermetidae fragments (95), black and yellowish orange pellets (5)	Fragments of barnacles and bivalves (90), echinoid spines (5), ferruginous-phyllossilicate grains (5)	Fragments of vermetidae and other gastropode (70), barnacle (20), foraminifera (2), red algae (2), bivalve (2) and echinoderm (2), and yellowish and black pellets (2)
	Size	Coarse silt to coarse sand	Fine to coarse sand	Very fine sand to granule	Very fine to median sand
	Fabric	Like the terrigenous	Between and inside the tubes	Scattered among the terrigenous	Scattered among the terrigenous
Clayey matrix	**Proportion (%)**	**58**	**2**	**3**	**14**
	Description	Micrite in two generations	Micrite	Micrite	Micrite in two generations
	Fabric	Partial filling of inter and intra grain pores, locally forming menisci	Partial filling, sometimes apparently geopetal, of some of the vermetidae chambers	Partial filling of inter and intra grain pores, locally forming menisci	Partial to complete filling of inter and, mainly, intratube pores,

					sometimes forming geopetal, pendular or meniscal fabrics
Cement	**Proportion (%)**	**1**	**1**	**2**	**1**
	Description	Phyllosilicate as coatings and menisci in clasts (50), and patches of iron oxyhydroxide amid micrite (50)	Clay-ferruginous coating with a particulate appearance around the clasts	Clay-ferruginous coating and meniscus	Post-micrite anisopaque fringe rimming part of the intratube pores
Porosity	**Proportion (%)**	**10**	**55**	**50**	**25**
	Description	Intergrain (60), intramatrix elongated (35) and growth framework (5)	Growth framework (60) and intergrain (40)	Intergrain (80) and growth framework (20)	Intergrain (65), growth framework (15), intragrain (10) and intramatrix elongated (5)
Depositional fabric		Growth framework with intense partial filling by micrite and, subordinately, terrigenous sand	Growth framework with partial filling by terrigenous and bioclastic sand and rare micrite	Growth framework with partial filling by terrigenous sand and rare micrite	Growth framework with intense partial filling by terrigenous sand, micrite and, subordinately, bioclasts

413

The bioconstruction framework was dominated by *P. varians* (65 to almost 100%) in all samples. Its other components, in order of decreasing mean abundance, were *T. stalactifera* (Pnh2 and Pnh5; Figs. 6C, 6D, 7D, 8A and 8B), *L.* af. *bisulcatus* (PCIM, Pnh2, Pnh5; Figs. 6A and 8D), red algae (Pnh5; Fig. 8C), bryozoan (PA; Figs. 6B and 9B), vestiges of plants (PA; Fig. 7B), encrusting foraminifera (Pnh5; Fig. 8E), other gastropods, with dimensions approximately three times smaller than *P. varians* (PCIM, Pnh5; Figs. 7A and 9B), and microbial mat (Pnh5; Fig. 8F). Although *T. stalactifera* occupies a limited volume (<20%) of the bioconstructions studied under the magnifying glass, its carapace is, in the lamellae, more robust and massive than that of the vermetid, which favored its representation in area in the two thin sections in which it was found. The low representation of *L.* af. *bisulcatus* as a bioconstruction component in the thin sections (maximum 5%) is due to its dispersed occurrence and thinner shell.

The walls of each tube of *P. varians* were generally anisopaque. They are formed by several concentric layers of prismatic/fibrous aragonite crystals, whose orientation can vary, in the same tube, between radial, inclined or tangential in relation to the circumference of the tube (e.g. Fig. 10A). The radial orientation was the dominant one. Intercalation, in the same tube wall, between orange to light brown colored laminae and others of white or beige color was frequently observed in the thin sections (Fig. 9D). The color was more common in the most superficial laminae of the tube. Dark brown colored laminae were also found, these exclusively on the outer edge (Fig. 7A, 8A, 8D and 9A). Locally, associated with this darkened surface of the tube, a cracked appearance and indentations suggestive of corrosion, or more likely, mechanical breakage, were observed (Fig. 9D). Concave-convex contacts of the dark brown surface with quartz grains were also observed (Fig. 10A).

The clastic components were dominated by terrigenous materials (5 to 20% of the rock), mainly quartz, with a subordinate presence of intraclasts (1 to 7%), which were formed by carbonate bioclasts (all samples, e.g. Fig. 9A), black or yellowish-orange pellets (PA, Pnh5; Fig. 9B) and grains of phyllosilicate and/or ferruginous composition similar to that of cements (Pnh2, e.g. Fig. 7C). Quartz grains engulfed by vermetid carbonate indicate contemporaneity between shell growth and terrigenous deposition. Among the bioclasts, the presence of vermetid fragments (PCIM, PA, Pnh5), and of bivalves, barnacles and echinoderms (Pnh2, Pnh5) larger than the average clasts in general (fine to very fine sand) was common. Locally, terrigenous grains filling vermetid tubes showed normal grading (Pnh2) or geopetal filling pattern (Pnh5).

The micritic matrix was found in the form of partial filling of inter and intragrain pores, in variable proportions (2 to 58%), and may present more than one texture and/or color (PCIM, Pnh5; Fig. 10C). Among the fabrics found, the menisci between the grains or between the adjacent walls of the bioconstruction (PCIM, Pnh2, and Pnh5), the pendular drip (Pnh5; Fig. 10D) and the geopetal filling (PA, Pnh5; Fig. 10C) stand out.

The post-micrite cement observed in the four samples is divided into non-carbonate and carbonate. The non-carbonate cement, with a cryptocrystalline texture, was found in small quantities (1 to 2%) in three of the analyzed samples (PCIM, PA, Pnh2; Figs. 7B and 7C). It is formed by phyllosilicates, iron oxyhydroxides or by an intimate association between these two compositions, that is, a clay-ferruginous material. Phyllossilicates

and clay-ferruginous material were observed in the form of coatings around the grains or lining pores (Fig. 7B) or as menisci between grains of fine sand to coarse silt. The oxyhydroxides appeared forming spots (up to 80 μm) or filling elongated pores in the middle of the micrite. The phyllosilicate cement presented an orange first-order interference color, an optical characteristic more compatible with clay minerals from the illite or smectite group. The presence of Si, Al, Mg and Fe, detected by SEM-EDS analysis of this cement (Toniolo, 2017), is indicative of smectite composition.

Carbonate cement, in the form of anisopaque microspar fringe, was found in one sample (Pnh5), lining part of the vermetidae chambers (Fig. 10D) or intergrain porosity. Cement grains are also embedded in the micrite. The external anisopaque coating of thin carbonate observed in sample PA (Fig. 9B) showed a microperforated texture, similar to that of the bryozoan found in this same thin section and detected by magnifying glass (Fig. 6B). Therefore, it must be a biogenic encrustation and not a cement stricto sensu.

Porosity between the clasts filling the bioconstruction (e.g. Figs. 8A and 8D) reach 60 to 80% in area. In the micrite-rich samples, secondary porosity consist of irregular or elongated and slightly sinuous voids within the micrite itself (Figs. 7A and 10C). To a lesser extent, subcircular perforations measuring up to 500 μm in the carbonate of vermetid shells were also observed, both in reflected light stereomicroscopic examination (Fig. 6B) and in transmitted light thin sections (Figs. 8E and 10B). Some of these perforations appear partially filled with micrite.

5. Discussion

5.1. Comparison between ages and implications for sea-level histories

The radiocarbon ages obtained from fossil shells and shell fragments of different species from the bioconstructions are in agreement with the relative ages expected based on the spatial relationship observed between them. The *T. stalactifera* shells are older than the overgrown vermetids shells, and the *L.* af. *bisulcatus* shells in life position, which perforate the bioconstruction, are younger (Table 1). At sample Pnh2 the ages also correspond to the living sequence inferred from the sample observation. First, *T. stalactifera* fixed on the bare rock at 6,260-5,943 ^{14}C cal aBP; thereafter *P. varians* built the bioconstruction at 5,894-5,604 ^{14}C cal aBP and finally the *L.* aff. *bisulcatus* bored the bioconstruction at 5,575-5,321 ^{14}C cal aBP. It stands out that the *P. varians* aliquot was obtained from the sample basal zone, next to the *T. stalactifera* shells.

The ages of individual shells are older than those obtained by dating bulk vermetid bioconstructions, and this difference increases with the age. The difference between the bioconstruction and the *P. varians* shell ages is around four centuries for the younger shells and reaches three thousand years for the older ones (Table 1 and Fig. 11). Considering the middle ages (e.g. 6,718.5 years for a 6,781-6,556 ^{14}C cal aBP interval), the two older *P. varians* shells (6,781-6,556 ^{14}C cal aBP and 5,894-5,604 ^{14}C cal aBP), are 82% and 36% older than the bulk bioconstruction age (3,897-3,499 ^{14}C cal aBP and 4,501-3,936 ^{14}C cal aBP, respectively). The two younger *P. varians* shells (1,405-1,302 ^{14}C cal aBP and 2,719-2,367 ^{14}C cal aBP) present ages 51% and 12% older, respectively, than the age given by the bulk bioconstruction. In the case of Pnh2 sample, the age difference is within the dating error margin: the *P. varians* shell gives age of 2,719-2,367 ^{14}C cal aBP

and the bulk bioconstruction, 2,489-2,063 ^{14}C cal aBP. These differences imply a great impact on the reliability of relative sea-level curves built from bulk samples, generally dated by the conventional radiocarbon method.

Considering the paleo-sea levels obtained in previous works for the four samples (Angulo, 1992; Angulo et al., 2002, 2006, 2022a) and using the revised ages reported here (Table 1), we infer that a Holocene highstand, more than 2 m above present level, occurred between 7,000 cal and 5,000 cal BP aBP (Fig. 11). This age is older than postulated in former works (e.g. Martin et al. 2003; Angulo et al. 2006, 2022a), which consider that post-glacial relative sea level (RSL) reached a level similar to the present one around 7,000 cal BP. In addition, as the post-glacial RSL maximum in former works was inferred from ages obtained from dating bulk samples (e.g. Martin et al. 2003; Angulo et al. 2006, 2022a), and the bulk samples could give younger ages (Table 1), we consider that the post-glacial maximum could be older than previously postulated. The differences in ages between bulk and individual shell samples highlight that paleo-sea levels inferred from bulk vermetid remains and respective Holocene sea-level curves need revision. This revision is especially important for the Mid-Holocene ages where the differences between bulk and individual shell samples are larger. Identification of the timing of the Mid-Holocene highstand is critical for testing models of glacio-isostatic adjustment (Woodroffe, 2009; Creel et al., 2024), for the understanding of coastal evolution, and for determining the role of sea-level in human settlement patterns (e.g. Giannini et al. 2010, Alessandretti et al. 2023). More data for separate species are therefore necessary to improve the accuracy of Holocene sea-level curves from Brazil.

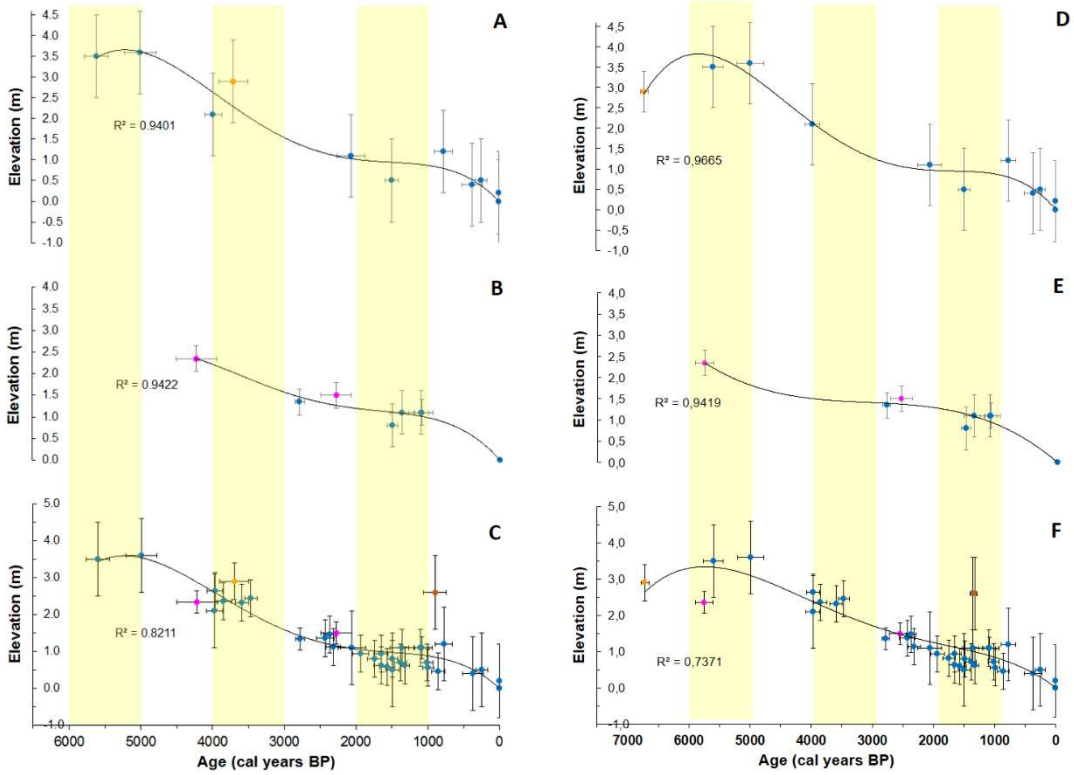

Fig. 11: Relative sea-level reconstructions from Angulo et al., 2022a (A,B,C)) and the data presented here (D, E, F), with their respective polynomial curves: A and D, Paraná; B and E, Ponta do Papagaio, Santa Catarina; C and F, Southern Brazilian coast north of

latitude 28°S. Colored points allow comparison between the previous dates of the bulk bioconstruction (A,B,C) and the new ones from individual vermetid samples (D,E,F): A, C, D, F correspond to 4th-order and B, E to 3rd-order polynomial curves. In constructing the curves, current sea level (0,0) was considered as an additional data point.

The sequence of the bioconstruction building by the different species – first *T. stalactifera*, subsequently *P. varians* and finally *L.* af. *bisulcatus* – observed in the samples and confirmed by the dating (Figs. 2 to 5 and Table 1) could be attributed to biological competition with stable or rising sea-level.

The sequence observed in the older bioconstructions (PCIM and Pnh5, Table 1) may correspond to a rising sea level, because the species living at lower levels (*P. varians*) is younger and superimposed on the one living at higher levels (*T. stalactifera*) (Laborel, 1979; Angulo and Souza, 2014; Angulo et al., 2022a; Pardal et al., 2023). This hypothesis is reinforced by the fact that the ages obtained from both species cover a period when RSL was supposedly rising (Fig. 11). However, the biological zone vertical extents of these two species partially coincide. Therefore, the alternative hypothesis that the recorded succession of building organisms may also result from biological competition under stable sea levels cannot be entirely ruled out. This hypothesis is best evaluated by examining the possibilities of differential rejuvenation of the ^{14}C ages of the two species by contaminants.

5.2. Characteristics of bioconstruction and its implications for paleo-sea level dating

The thin sections studied demonstrated that *P. varians* appears associated with several other organisms, some of them younger and/or from another biological zone. In view of that, knowing its typical shapes in flat section is important to allow high-precision collections of this species aimed at reconstructing the marine paleolevel. The four different two-dimensional shapes (spiral or concentric, cloverleaf, subcircular to oval, and dumbbell-like) observed in vermetid chambers result from distinct viewpoints or thin section orientations. They can be understood based on the description of the three-dimensional geometry of the shell of *P. varians* (Laborel, 1986) and other species of this genus (Savazzi, 1996; Scuderi, 2012). The two-dimensional shape depends basically on the orientation of the section in relation to the tube and whether or not this section cuts the axis of winding or columella, and in what relative direction. Thus, the spiral or concentric shape appears when the columella is sectioned transversely, and the tubes, longitudinally; the cloverleaf shape is due to the presence of a pair of internal laminae projecting from the columellar wall; therefore, it occurs when the columella is sectioned longitudinally (Fig. 9A); the subcircular and oval shapes (Figs, 6A and 6B) are found when the section is transversal or oblique to the tube, respectively, but without sectioning the columella; finally, the shape similar to a bean or dumbbell (Fig. 7A) also appears in sections that do not cross the columella, but are longitudinal to the tube.

The dark brown outer rim, recorded in part of the vermetid carapaces in all samples studied (Figs. 7A, 8A, 8B, 8D and 9A), suggests some form of weathering or eodiagenetic alteration of aragonite in more prolonged contact with the atmosphere, seawater or microbial communities. It is identical to the micritic envelopes sensu Gvirtzman and

Friedman (1977), widely described in carbonate grains of Phanerozoic deposits, and is therefore interpreted as such here. Micritic envelopes are produced in eodiagenesis by endolithic microbes deposited in the photic zone (Bathurst, 1966; Calvet, 1982; Perry, 1999) and can be destructive or constructive in origin (Kobluk and Risk, 1977; Calvet, 1982; Reid and Macintyre, 1998, 2000; Perry, 1999; Ge et al., 2020). In the case of aragonite substrate, as attested in Holocene examples, the alteration implied by micritic envelope formation may include neomorphism to high Mg calcite (Kendall and Patrick, 1969; Scherer, 1974; Reid et al., 1992; Reid and Macintyre, 1998). This neomorphism may indicate changes in the chemical composition of the carbonate in terms of Mg and trace element content (e.g. Sr and Pb), as well as in the ratios between stable isotopes of O and C; it may also indicate formation of the carbonate after the vermetid's lifetime, especially if it is a constructive envelope, thus having possible implications for the interpretation of the dating result.

On the other hand, the micritic envelope found in the samples studied is generally not very expressive in volume, with rare exceptions (Fig. 9A); this means that in most cases the difference in age of a sample dated from the whole shell, with envelope, in relation to the original aragonite from the vermetid shell, without the envelope, may be small, likely within the error margin of the dating method.

In the samples studied, both the presence and thickness of the micritic envelope can vary, even in adjacent chambers of the same thin section (e.g. Figs. 9A and 9D). Considering that the formation of the envelope presupposes exposure of shell aragonite to water, this suggests alternation between phases and/or preferential growth sites of the vermetid carbonate. In some cases, the periphery of the chamber with micritic envelope is partially surrounded by another layer of aragonite, with little or no micritic envelope (Fig. 9D). This apparently points to the interruption of growth, marked by the exposure and alteration of the chamber edge, followed by a new growth phase.

Fracturing and indentations at the edge of vermetid chambers with micritic envelope (Fig. 9D) may result from the creation of planes of weakness in the aragonite crystals due to the recrystallization force during neomorphism. The close adhesion of rigid quartz grains, in concave-convex contacts with the surface of the vermetid containing a micritic envelope (Fig. 10A), indicates that envelope carbonate had ductile or plastic behavior. This rheology is consistent with the growth of biofilms on the carbonate surface, a phenomenon described in the formation of constructive micritic envelopes (Ge et al., 2020).

The dominance of quartz and other terrigenous elements among the clastic components is consistent with the mineralogy of the beaches adjacent to the cliffs where the bioconstructions were collected. The intraclastic components, on the other hand, reflect the sessile benthic community existing on the cliff. Two specific types of intraclasts indicate mechanical reworking of the bioconstructed framework and respective cement. They are: fragments of gastropods, bivalves and barnacles with a coarser grain size than the average of the clasts (Figs. 9A and 9B); and grains with phyllosilicate and/or ferruginous composition similar to that of the cement coating the chambers (Fig. 7C). These kinds of intraclasts would have been formed by fragmentation during the breaking of waves against the bioconstruction, with immediate redeposition in its pores.

The frequent presence of geopetal patterns in the chambers filled with matrix (Fig. 10C) or sand clasts (Fig.8D) suggests that the entry of this material occurred under conditions of non-saturation in water (vadose) (e.g. Tucker and Wright, 1990; Scholle and Ulmer-Scholle, 2003; Flügel, 2010; Hood and Wallace, 2012), therefore above the mean tide level. Fabrics of micritic matrix in meniscus and pendular (Fig. 10D) reinforce this interpretation. Given that *P. varians* lives essentially underwater, it is likely that most of this vadose filling occurred with RSL lower than that of the animal's lifetime. In this regard, the large variation in micrite content (2 to 58%) in the studied bioconstructions may in part be linked to the time of action of vadose processes. In theory, the higher the paleo-sea level of the bioconstruction, the longer the time of action of these processes and the greater the probability of filling by micritic matrix. In fact, of the three samples indicating RSL greater than 2.0 m above present, two (PCIM and Pnh5) presented the highest micrite contents found (58 and 14%, respectively). There were two phases of micrite filling, at least in sample Pnh5, where a generation of thinner micrite fills pores left by the previous generation, including in a geopetal pattern (Fig. 10C). The interpretation of more than one phase of pore filling by micrite is reinforced by the fact that the microspar cement fringe which coats the intratube filling of pendulous micrite (Fig. 10D) also occurs reworked amid this thinner intergrain micrite.

Coatings, menisci and pore linings of ferruginous clay material (Fig. 7B) and stains and elongated pore-filling of iron oxyhydroxides point to prolonged oxidizing conditions, arising after the significant lowering of the RSL in which the bioconstruction organisms lived. Those materials are relatively late in the post-depositional history, as suggested by the fact that they fill narrow, sinuous and elongated pores, attributed to bioturbation of the intra-tube micrite filling; moreover, they are concentrated on the top of the bioconstruction. The supposed microbial mat in Pnh5 appears on the top of this iron oxyhydroxide cement, and is therefore even younger. In view of the flat laminar fabric, it is assumed to correspond to a smooth microbial mesostructure of tufa microbialite (e.g. Smith et al., 2011; Edwards et al., 2017; Garner et al., 2024) and to have therefore developed under inter- to supratidal conditions, with occasional influence from sea spray.

All impurities listed here are more common in vermetids than in barnacles, which may be related to the aragonitic composition of the former. They are also more difficult to avoid during sampling in vermetids, due to the small size of their tubules and the larger specific surface available for filling, cementation or adhesion by contaminants. Furthermore, as observed in this study, vermetids are more prone than barnacles to the formation of micritic envelopes, perhaps due to their aragonitic composition and/or because they compose the part most exposed to light in the bioconstructions studied, where they appear wrapped around *T. stalactifera*.

In view of that, the younger ages given by ^{14}C conventional dating of large vermetid bioconstruction samples can be, thererore, attributed to several factors, as cementation, carbonate neomorphism and late biofouling. Toniolo et al. (2020) alert that to obtain confident ages from vermetid samples is necessary to avoid contamination by cements and clay minerals containing organic matter from the samples. To get around this problem, they recommend, and adopt, the following succession of treatments: (a) clean the surface sample with a brush under flowing water, (b) immerse the sample in H_2O_2, 30 volumes, for at least 48 h, (c) disaggregate the

colonies mechanically, and (d) select fragments of vermetid shells under stereoscopic microscope.

However, even these selected vermetid shell fragments may still contain impurities. This happens because some of the impurities reported here in vermetid shells may be imperceptible to the hand lens or magnifying glass, and therefore impossible to avoid during collection. The micritic envelope is the most difficult to be detected, but micrite and microspar cement coatings, adhesion of bryozoans and microbial mats, as well as the presence of rootlets, may also be subtle and go unnoticed. Therefore, the use of bioconstructions as RSL indicators should ideally be accompanied or even preceded by analysis of thin sections under an optical microscope. The best solution is collection with visual control under a microscope in real time, using, for example, high-precision microdrills or micromills, with diameter of 100 µm or smaller. Once the powder or particles have been collected by this or another method, the concentration of the vermetid's original aragonite by density (Araujo et al. 2021) can also be useful. This helps avoid the inclusion of particles rich in secondary calcite or other light impurities in the material to be dated.

6. Conclusion

Vemetid gastropods biocostructions are a critical paleo-sea level indicator along many rocky shorelines globally, including the Brazilian coastline. We conclude that there are significant age discrepancies between radiocarbon ages derived from bulk vermetid bioconstruction remains and the shells of the different species that constitute the bioconstruction. The age difference is larger in older bioconstructions and implies a significant impact on the reliability of RSL curves built from samples dated by bulk vermetid remains. Consequently, ages of paleo-sea levels inferred from bulk vermetids remains and respective Holocene sea-level curves need revision. This revision is especially important for the Mid-Holocene ages, where the differences are larger. For example, the new species-specific radiocarbon ages presented here indicate that the the Holocene RSL was > 2m above present level around 7,000 cal aBP, while former works postulate that, at that time sea level was similar to the present one. More data are necessary to improve the accuracy of Holocene sea-level curves for the Brazilian coast, which are heavily based on ages of bulk vermetid bioconstructions.

We also conclude that to improve the Holocene paleo-sea levels ages, close inspection of samples is recommended to avoid carbonate neomorphism and contamination by other carbonate or carbonaceous materials such as cements, micrite envelope, rootlets and microbiofoulings.

Acknowledgments

We are grateful to the Brazilian Research Council (CNPq) for their financial support though projects numbers 557141/2009-5, 457714/2013-1, 307055/2013-2, 442865/2015-5, 428341-2018-7, 443254/2019-2 and 403552/2024-9, as well as to Fundação de Amaro à Pesquisa no Estado de São Paulo (FAPESP, process 09/54232-4) and UK Research and Innovation (UKRI, grant NE/Y003187/1). RJA, PCFG and MCS are sponsored by CNPq fellowships (311837/2022-0, 304866/2022-9, 314836/2023-3) and

JASR by CAPES scholarship (88887.132637/2025-00). TFT was sponsored by CAPES and FAPESP (13/21941-8).

References

Alessandretti, L., Giannini, P.C.F., Warren, L., Brückmann, M.P., Martini, A. 2023. Earth, wind and fire: Interactions between Quaternary environmental dynamics and human occupation on the southern coast of Brazil. Quaternary Science Reviews, 301, p. 107950, 2023.

Angulo, R.J., 1989. Fossil vermetidae between latitudes 25°34'S and 27°09'S, state of Paraná and state of Santa Catarina, Brazil. International Symposium on Global Changes in South America during Quaternary 1:263-268. Special Publication.

Angulo, R.J., 1992. Geologia da Planície Costeira do Estado do Paraná. Ph.D. Thesis, Instituto de Geociências, Universidade de São Paulo, 332 p. (in Portuguese).

Angulo, R.J., 1993. Indicadores biológicos de paleoníveis marinhos quaternários na costa paranaense. Boletim Paranaense de Geociências, 41:1-34. (in Portuguese).

Angulo, R.J., Souza, M.C., 2014. Conceptual review of Quaternary coastal paleo-sea level indicators from Brazilian coast. Quaternary and Environmental Geosciences, 5(2):1:32 (in Portuguese).

Angulo, R.J., Lessa, G.C., 1997. The Brazilian sea level curves: a critical review with emphasis on the curves from Paranaguá and Cananéia regions. Mar. Geol. 140: 141-166.

Angulo, R.J., Giannini, P.C.F., Suguio, K., Pessenda, L.C.R., 1999. Relative sea-level changes in the last 5.500 years in southern Brazil (Laguna-Imbituba region, Santa Catarina state) based on vermetid 14C ages. Marine Geology 159, 323:339.

Angulo, R.J., Borzone, C.A., Noernberg, M.A., Quadros, C.J.L, Souza, M.C., Rosa, L.C., 2016. The State of Paraná beaches. In: Short A.D., Klein, A.H.F. (eds.) Brazilian Beach Systems. Coastal Research Library 17, Springer, Dordrecht, pp. 419-464. DOI 10.1007/978-3-319-30394-9_16.

Angulo, R.J., Pessenda, L.C.R., de Souza, M.C., 2002. O significado das datações ao 14C na reconstrução de paleoníveis marinhos e na evolução das barreiras quaternárias do litoral paraense. Rev. Bras. Geociências 32:95-106 (in Portuguese).

Angulo, R.J., Lessa, G.C., Souza, M.C., 2006. A critical review of mid- to late-Holocene Sea-level fluctuations on the eastern Brazilian coastline. Quaternary Science Reviews 25:486–506.

Angulo, R.J., Lessa, G.C., Souza, M.C., 2009. The Holocene barrier systems of Paranaguá and northern Santa Catarina coasts, Southern Brazil. In: In: Dillenburg, S.R. & Hesp, P.A. ed. Geology and Geomorphology of Holocene Coastal Barriers of Brazil. Berlin – Heidelberg, Springer, p. 135-176.

Angulo, R.J., Souza, M.C., Campos, T.F.C., Bezerra, F.H.R., Fernandes, L.A., Giannini, P. C.F., Pitombo, F.B., Veiga, F.A., 2013a. Evidence for Late Quaternary episodic

748 uplift of the São Pedro and São Paulo Archipelago, Equatorial Atlantic.
749 Quaternary International 317, 102–111.

750 Angulo, R.J., Souza, M.C., Fernandes, L.A., Disaró, S.T., 2013b. Quaternary sea-level
751 changes and aeolianites in the Fernando de Noronha archipelago, northeastern
752 Brazil. Quaternary International 305, 15–30.

753 Angulo, R.J.; Souza, M.C., Müller, M.E.J.; Noernberg M.A.; Oliveira L.H.S.; Soares C.R.;
754 Borzone C.A.; Marone E.; Quadros C.J.L., 2018. Paraná. In: Muehe, D. (org.).
755 *Panorama da erosão costeira no Brasil*, Ministério do Meio Ambiente, pp. 586-
756 640 (in Portuguese).

757 Angulo, R.J., Souza, M.C., Giannini, P.C.F., Dillenburg, S.R., Barboza, E.G., Rosa, M.L.C. C.,
758 Hesp, P.A., Pessenda, L.C.R., 2022a. Late-Holocene sea levels from vermetids and
759 barnacles at Ponta do Papagaio, 27º 50'S latitude and a comparison with other
760 sectors of southern Brazil. Quaternay Science Reviews, 286(202) 107536.

761 Angulo, R.J., Souza, M.C., Rosa, M.L.C.C., Barboza, E.G., Fernandes, L.A., Guedes, C.C.F.,
762 Oliveira, L.H.S., Manzolli, R.P., Disaró, S.T., Ferreira, A.G., Martin, C.M., 2018b.
763 Trindade. Quaternary sealevel changes and coastal evolution of the Island of
764 Trindade, Brazil. J. S. Am. Earth Sci. 84, 208–222.

765 Angulo, R.J., Souza, M.C., Rosa, M.L.C.C., Barboza, E.G., Lessa, G.C., Pessenda, L.C.R.,
766 Ferreira Júnior, A.L., 2022b. Late Mid- to Holocene sealevel changes at Abrolhos
767 Archipelago and Bank, southwestern Atlantic. Brazil. Marine Geology, 450 (2022)
768 106841.

769 Angulo, R.J., Souza, M.C., Rosa, M.L.C.C., Caron, F., Barboza, E.G., Costa, M.B., Macedo,
770 E., Vital, H., Gomes, M.P., Garcia, K.B.L., 2022c. Paleo-sea levels, Late-Holocene
771 evolution, and a new interpretation of the boulders at the Rocas Atoll,
772 southeastern Equatorial Atlantic. Marine Geology, 447(2022) 106780.

773 Araujo, J.C., Macario, K.C.D., Moreira, V.N., dos Santos Passos, A., Jesus, P.B., Seoane,
774 J.C.S., Dias, F.F. 2021 Bioindicators of sea-level fluctuations in southeastern
775 Brazil: new data and methodological review. Radiocarbon. 63(4): 1149-1163.
776 doi:10.1017/RDC.2021.50

777 Bathurst, R.G.C., 1966. Boring algae, micrite envelopes and lithification of molluscan
778 biosparites. Geol. J. 5, 15–32.

779 Breves, A., Széchy, M.T.M., Lavrado, H.P., Junqueira, A.O., 2017. Abundance of the
780 reefbuilding Petaloconchus varians (Gastropoda: Vermetidae) on intertidal rocky
781 shores at Ilha Grande Bay, southeastern Brazil. An. Acad. Bras. Cienc. 89 (2), 907–
782 918.

783 Calvet, F., 1982. Constructive micrite envelope developed in vadose continental
784 environment in Pleistocene eoliantes of Mallorca (Spain). Acta Geológica
785 Hispánica 17, 169–178.

786 Choquette, P.W., Pray, L., 1970. Geologic nomenclature and classification of porosity in
787 sedimentary carbonates. AAPG Bull., 54: 207-250.

788 Creel, R.C., Austermann, J., Kopp, R.E., Khan, N.S., Albrecht, T. and Kingslake, J., 2024.
789 Global mean sea level likely higher than present during the holocene. Nature
790 communications, 15, 10731.

791 Dominguez, J.M.L., 2009. The coastal zone of Brazil. In: Dillenburg, S.R. & Hesp, P.A.
792 (orgs.) Geology and Geomorphology of Holocene Coastal Barriers of Brazil.
793 Lecture Notes in Earth Sciences, vol. 107. Springer-Verlag, Berlin, pp. 17-51.

794 Donnarumma, L., D'Argenio, A., Sandulli, R., Russo, G.F., Chemello, R., 2021. Unmanned
795 aerial vehicle technology to assess the state of threatened biogenic formations:
796 The vermetid reefs of mediterranean intertidal rocky coasts. Estuarine, Coastal
797 and Shelf Science, 251, 107228.

798 Edwards, M.J.K., Anderson, C.R., Perissinotto, R., Rishworth, G.M., 2017. Macro- and
799 meso-fabric structures of peritidal tufa stromatolites along the Eastern Cape
800 coast of South Africa. Sediment. Geol., 359: 62–75,
801 https://doi.org/10.1016/j.sedgeo.2017.08.006, 2017.

802 Flügel, E., 2010. Microfacies of Carbonate Rocks: Analysis, Interpretation and
803 Implications, vol 2. Springer, Berlin

804 Garner, T.W., Andrew, J., Cooper G., Smith, A.M., Rishworth, G.M., Forbes, M., 2024.
805 Reviews and syntheses: Tufa microbialites on rocky coasts – towards an
806 integrated terminology. Biogeosciences, 21: 4785–4807.
807 https://doi.org/10.5194/bg-21-4785-2024

808 Giannini, P.C.F., Sawakuchi, A.O., Martinho, C.T., Tatumi, S.H., 2007. Eolian depositional
809 episodes controlled by Late Quaternary relative sea level changes on the Laguna-
810 Imbituba coast, South Brazil. Marine Geology, 237(2007): 143-168.

811 Giannini, P.C.F., Guedes, C.C.F., Nascimento, D.R. Jr., Tanaka, A.P.B., Angulo, R.J., Assine,
812 M.L., Souza, M.C., 2009. Morphology and sedimentology of Ilha Comprida,
813 southern São Paulo coast. In: Dillenburg, S.R. & Hesp, P.A. ed. Geology and
814 Geomorphology of Holocene Coastal Barriers of Brazil. Berlin – Heidelberg,
815 Springer, p.177-224.

816 Giannini, P.C.F., Villagran, Ximena S., Fornari, M., Nascimento Jr., D.R., Menezes, P.M.L.,
817 Tanaka, A.P.B., Assunção, D., Deblasis, P., Amaral, P.G.C. 2010. Interações entre
818 evolução sedimentar e ocupação humana na costa centro-sul de Santa Catarina,
819 Brasil. Boletim do Museu Paraense Emílio Goeldi. Ciências Humanas, 5: 105-128.

820 Gvirtzman, G., Friedman, G.M., 1977. Sequence of progressive diagenesis in coral reefs.
821 In: Frost, H., Weis, M.P., Saunder, J.B. (Eds.), Reef and Related Carbonates:
822 Ecology and Sedimentology. Studies in Geology AAPG, pp. 357–380 No.4.

823 Heaton T.J., Köhler P., Butzin M., Bard E., Reimer R.W., Austin W.E.N., Bronk Ramsey C.,
824 Hughen K.A., Kromer B., Reimer P.J., Adkins J., Burke A., Cook M.S., Olsen J.,
825 Skinner L.C., 2020. Marine20-the marine radiocarbon age calibration curve (0-
826 55,000 cal BP). Radiocarbon 62. doi: 10.1017/RDC.2020.68.

827 Hesp, P.A., Giannini, P.C.F., Martinho, C.T, Silva, G.M., Asp Neto N.E., 2009. The
828 Holocene barrier system on the Santa Catarina coast, southern Brazil. In:
829 Dillenburg, S.R. & Hesp, P.A. (orgs.) Geology and Geomorphology of Holocene

Coastal Barriers of Brazil. Lecture Notes in Earth Sciences, vol. 107. Springer-Verlag, Berlin, pp. 93-133.

Hood, A.V.S., Wallace M.W., 2012. Synsedimentary diagenesis in a Cryogenian reef complex: ubiquitous marine dolomite precipitation. Sediment Geol. 324: 12–31

Kempf M., Laborel J., 1968. Formations de vermets et d'algues calacaires sur lês côtes du Brésil. *Recueil des Travaux de la Station Marine d'Endoume*, 59(43)325-435.

Kendall, C.G.S.C., Patrick, A., 1969. Holocene shallow-water carbonate and evaporate sediments of Khor al Bazam, Abu Dhabi, southwest Persian Gulf. AAPG Bulletin 53, 841–869.

Kobluk, D.R., Risk, M.J., 1977. Micritization and carbonate-grain binding by endolithic algae. AAPG Bull. 61, 1069–1082.

Laborel J., 1969. Les pouplements de madréporaires des côtes tropicales du Brésil. *Annales de l'Universtité D'Abidjan*, Serie EII Fascicule 3, Ecologie. 261p.

Laborel, J., 1977. Are reef building vermetid disappearing in the South Atlantic? Proc. Int. Coral Reef Symposium 3, 233–237.

Laborel, J., 1979. Fixed marine organisms as biological indicator for the study of recent sea level and climatic variations along the Brazilian tropical coast. In: Proceedings International Symposium on: Coastal Evolution in the Quaternary, Sao Paulo, 1978. Proceedings, São Paulo, IGCP/Project 61, Instituto de Geociências. Universidade de São Paulo, pp. 193–211.

Laborel, J., 1986. Vermetid gastropods as sea-level indicators. In: Van de Plassche, O. (Ed.), Sea Level Research, a Manual for the Collection and Evaluation of Data. 12. Geo Books, Norwich, pp. 281–310.

Laborel, J., Kempf M., 1966. Formação de vermetos e algas calcárias nas costas do Brasil. Trabalhos do Instituto Oceanográfico da Universidade Federal de Pernambuco, 7/8:33-50 (in Portuguese).

Marone, E., Jamiyanaa, D. 1997. Tidal characteristics and a variable boundary numerical model for the M2 tide for the estuarine complex of the Bay of Paranaguá, PR, Brazil. Nerítica, 11(1-2):95-107.

Mineropar – Minerais do Paraná AS, 1989. Mapa geológico do Estado do Paraná. Departamento Nacional da Produção Mineral (DNPM), Brasília, 1map

Narchi, W., 1974. Functional morphology of Petricola (Rupellaria) typica (Bivalvia: Petricolidae). Marine Biology, 27:123-129.

Narchi, W., 1975. Functional morphology of a new Petricola (Mollusca Bivalvia) from the littoral of São Paulo, Brazil. In: Proceedings of the Malacological Society of London, 41(5):451-465.

Pardal, A., Martinez, A.S., Ciotti, Á.M., Christofoletti, R.A., Cordeiro, C.A., 2023. Macroecology of rocky intertidal benthic communities along the southwestern Atlantic: patterns of spatial variation and associations with natural and anthropogenic variables. Marine environmental research, 190, 106099.

870 Peres, J.M., Picard, J. 1964. Nouveau Manuel de bionomie benthique em Mer
871 Mediterranée. Recueil des Travaux de Station Marine d'Endoume, 4, 1.

872 Perry, C.T., 1999. Biofilm-related calcification, sediment trapping and constructive
873 micrite envelopes: a criterion for the recognition of ancient grass-bed
874 environments? Sedimentology 46, 33–45.

875 Pianca, C., Mazzini, P.L.F., Siegle, E., 2010. Brazilian offshore wave climate based on
876 NWW3 reanalysis. Brazilian Journal of Oceanography 58(1):53e70.

877 Picone, F., Chemello, R., 2023. Seascape characterization of a Mediterranean vermetid
878 reef: a structural complexity assessment. Frontiers in Marine Science, 10,
879 1134385.

880 Pittman, E.D., 1979. Porosity diagenesis and productive capability of sandstone
881 reservoirs. In: Scholle, P. A. & Schluger, P.R. eds. Aspects of Diagenesis. Society
882 Economic Paleontologists and Mineralogists Special Publication, 26, p. 159-173.

883 Powers, M.C., 1953. A new roundness scale for sedimentary particles. Jour. Sedim.
884 Petrol., 23: 117-119.

885 Reid, R.P., Macintyre, I.G., 1998. Carbonate neomorphism in shallow marine
886 environments: a widespread diagenetic process forming micritized grains. J.
887 Sediment. Res. 68, 928–946.

888 Reid, R.P., Macintyre, I.G., 2000. Microboring versus neomorphism: future insight into
889 the micritization process. J. Sediment. Res. 70, 24–28.

890 Reid, R.P., Macintyre, I.G., Post, J.E., 1992. Micritized skeletal grains in northern Belize
891 Lagoon; a major source of Mg-calcite mud. J. Sediment. Res. 62, 145–156.

892 Savazzi, E., 1996. Adaptations of vermetid and siliquariid gastropods. Paleontology
893 39:157-177.

894 Scherer, M., 1974. Submarine recrystallization of a coral skeleton in a Holocene
895 Bahamian reef. Geology 2, 499–500.

896 Scholle, P.A., Ulmer-Scholle, D.S., 2003. A Color Guide to the Petrography of Carbonate
897 Rocks: Grains, Textures, Porosity, Diagenesis. Am Assoc Petrol Geol, Tulsa

898 Scuderi, D., 2012. A new species of Petaloconchus Lea, 1843 from the Mediterranean
899 Sea (Mollusca, Gastropoda, Vermetidae). Biodiversity Journal, 3(2): 123-128.
900 https://www.molluscabase.org/aphia.php?p=sourcedetails&id=164233

901 Shennan, I., 2015. Handbook of sea-level research: framing research questions. In:
902 Shennan, I., Long, A.J., Horton, B.P., (Eds.). Handbook of Sea-level Research, John
903 Wiley & Sons, pp. 3-25.

904 Smith, A.M., Andrews, J.E., Uken, R., Thackeray, Z., Perissinotto, R., Leuci, R., Marca-Bell,
905 A., 2011. Rock pool tufa stromatolites on a modern South African wave-cut
906 platform: partial analogues for Archaean stromatolites? Terra Nova: 23, 375–
907 381, https://doi.org/10.1111/j.1365-3121.2011.01022.x, 2011.

908 Spotorno-Oliveira, P., Tamega, F.T.S., Bemvenuti, C.E., 2012. An overview of the recent
909 vermetids (Gastropoda: vermetidae) from Brazil. Strombus 19, 1e8.

910 Stephenson, T.A., Stephenson, A., 1949. The universal features of zonation between tide
911 marks on rocky coasts. Journal of Ecology, 37(2):289-305.

912 Stuiver, M., Reimer, P.J., 1993. Extended 14C Data Base and Revised CALIB 3.0 14C Age
913 Calibration Program. Radiocarbon, 35, 215-230. https://doi.org/
914 10.1017/S0033822200013904

915 Toniolo, T.F., 2017. Vermetídeos Fósseis como Indicadores da Variação do Nível Relativo
916 do Mar e de Possíveis Alterações na Circulação Costeira no Holoceno ao Longo
917 do Litoral Brasileiro. Master Thesis, Instituto de Geociências, Universidade de
918 São Paulo, 124 p. (in Portuguese).

919 Toniolo, T.F., Giannini, P.C.F., Angulo, R.J., Souza, M.C., Pessenda, L.C.R., Spotorno-
920 Oliveira, P., 2020. Sea-level fall and coastal water cooling during the Late
921 Holocene in southeastern Brazil based on vermetid bioconstructions. Marine
922 Geology, 428, 106281.

923 Tsang, L.M., Chu, K.H., Achituv, Y., Chan, B.K.K., 2015. Molecular phylogeny of the acorn
924 barnacle family Tetraclitidae (Cirripedia: Balanomorpha: Tetraclitoidea): Validity
925 of shell morphology and arthropodal characteristics in the systematics of
926 Tetraclitid barnacles. Molecular Phylogenetics and Evolution 82: 324–329.

927 Tucker, M.E., Wright, V.P., 1990. Carbonate Sedimentology. Blackwell, Oxford

928 Van-Andel, T.H., Laborel, J., 1964. Recent high relative sea level stand near Recife, Brazil.
929 Science 145, 580e581.

930 Wentworth, C.K., 1922. A scale of grade and class terms for clastic sediments. Journal of
931 Geology, 30: 377-392.

932 Wildner, W., Camozzato, E., Toniolo, J.A., Binotto, R.B., Iglesias, C.M.F., Laux, J.H., 2014.
933 Mapa Geológico do Estado de Santa Catarina, Escala 1:500.000, CPRM, Porto
934 Alegre, 2014.

935 Woodroffe, S.A., 2009. Testing models of mid to late Holocene sea-level change, North
936 Queensland, Australia. Quaternary Science Reviews, 28: 2474-2488.